ACS Chemical Neuroscience

pubs.acs.org/chemneuro Research Article

In Vitro and In Vivo Evaluation of Small-Molecule Disassemblers of Pathological Tau Fibrils

Hope Pan,[♦] Xinyi Cheng,[♦] Jeffrey Zhang,[♦] Ke Hou, Kevin A. Murray, Kapil Manglani, Cansheng Zhu, Hung-Kai Hsu, Marisa Mekkittikul, Tyler Halladay, Hilda Mirbaha, Gazmend Elezi, Romany Abskharon, Michael R. Sawaya, Alexander Bombino, Christopher K. Williams, Michael DeTure, Dennis W. Dickson, Harry V. Vinters, Julian P. Whitelegge, Patrick G. Harran, Gregory M. Cole, Sally A. Frautschy, and David S. Eisenberg*

Cite This: https://doi.org/10.1021/acschemneuro.5c00940 Read Online

ACCESS | Metrics & More | Article Recommendations | Supporting Information

ABSTRACT: Aggregation of the microtubule-binding protein tau is the histopathological hallmark of Alzheimer's disease (AD) and other neurodegenerative diseases, which are collectively known as tauopathies. Tau aggregation in AD patients is correlated with neuron loss, brain atrophy, and cognitive decline, and pro-aggregation tau mutations are sufficient to cause neurodegeneration and dementia in humans and tauopathy model mice. Thus, reversing tau aggregation is a potential therapeutic avenue for AD. In a previous study, we discovered CNS-11, a small molecule that disaggregates AD patient brain-extracted tau fibrils in vitro. In this study, we identify two chemical analogs of CNS-11, named CNS-11D and CNS-11G, that disaggregate AD patient brain-extracted tau fibrils and prevent seeding in a tau aggregation cell culture model. We also demonstrate that 8 weeks of treatment with either CNS-11D or CNS-11G reduces levels of insoluble tau in a mouse model of tauopathy. Our work defines the properties of two small molecules that diminish aggregation of tau in vivo and provides further support for structure-based methods to target tau for treatment of AD.

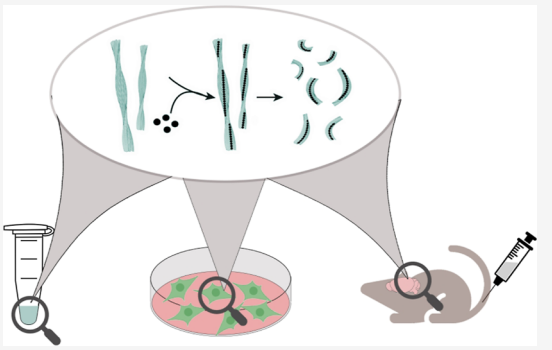

KEYWORDS: *neurodegenerative disease, Alzheimer's disease, tau, small molecules, disaggregation, mouse model*

INTRODUCTION

Alzheimer's disease (AD) is a slow and progressive form of dementia. AD is associated with the accumulation of proteins amyloid-β (Aβ) and tau as extracellular amyloid plaques and intracellular neurofibrillary tangles (NFTs), respectively. Amyloid plaques and NFTs are hypothesized to be neurotoxic; therefore, targeting their formation has been one approach for designing therapeutics. For example, FDA-approved drugs lecanemab and donanemab are monoclonal antibodies that target Aβ and the formation of amyloid plaques.[1,2] However, these drugs can only slow the progression of AD and cannot halt or reverse it. Laboratory and clinical studies in AD patients have demonstrated that increased NFTs formed from tau, not plaques formed from Aβ, are correlated with progressive neuron loss, brain atrophy, and cognitive decline.[3−11] Therefore, a drug targeting tau, either alone or in combination with a drug that targets Aβ, could have greater potential for halting the progression of AD.

NFTs form when soluble tau molecules adopt identical, tightly packed conformations that exclude solvent and stack into an insoluble amyloid fibril. In AD patients, tau deposition and NFT formation progress in an orderly fashion, beginning in the locus coeruleus and entorhinal cortex, spreading to synaptically connected regions such as the hippocampus, and eventually moving to the neocortex.[12,13] This pattern suggests that tau pathology spreads by "seeding" or fibril-templated conversion of soluble tau to its insoluble form by existing tau fibrils. Multiple laboratory studies have demonstrated seeding among cultured cells[14−17] and in mice.[18−23] When small quantities of preformed fibrils are transfected into tau-expressing cells, large amounts of soluble tau are rapidly recruited ("seeded") into insoluble aggregates resembling NFTs.[16] When transgenic mice expressing human tau are injected intracranially with preformed fibrils, tau inclusions develop in the injected hippocampus and eventually spread to the contralateral hippocampus.[20,21] Drugs that disaggregate insoluble tau fibrils and prevent them from seeding the

Received: December 2, 2025
Revised: December 11, 2025
Accepted: December 22, 2025

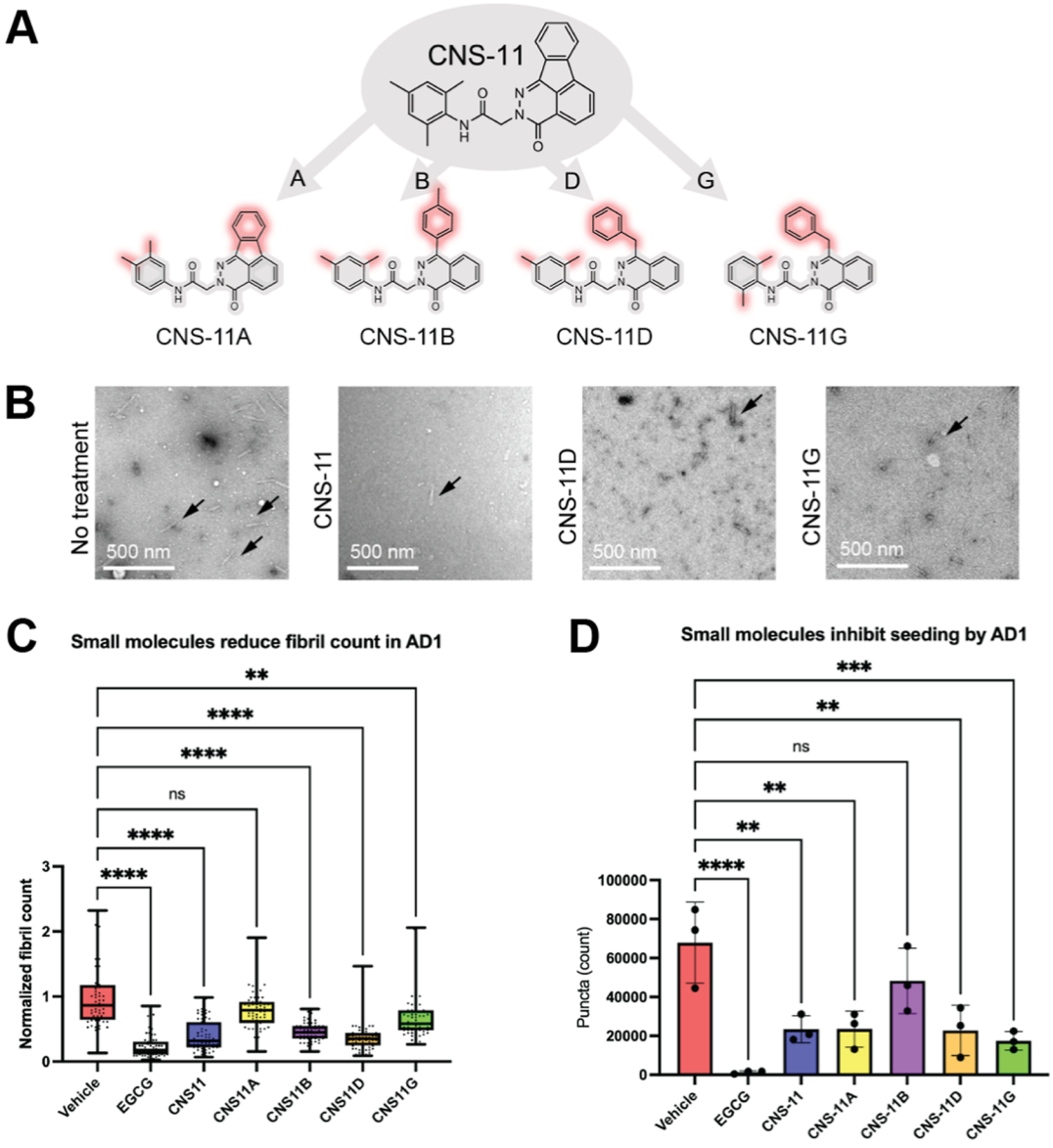

Figure 1. Chemical analogs of CNS-11 disaggregate tau fibrils from AD patients and prevent seeding in HEK293 biosensor cells. (A) Chemical analogs of CNS-11. Conserved chemical structures are colored in gray and distinctive chemical structures are colored in red. (B) Negatively stained electron micrographs of AD brain-extracted tau fibrils from AD1 after incubation for 24 h at 37 °C with no treatment, vehicle (1% DMSO), EGCG, CNS-11, or one of the four chemical analogs of CNS-11 at a concentration of 500 μM. (C) Quantification of AD brain-extracted tau fibrils (black arrows) present on EM images (n = 40 images taken from random points on the EM grid). Images were approximately 4× the size of images in (B). Statistical analysis was performed using a Kruskal–Wallis test followed by Dunn's multiple comparison test (ns, $P > 0.05$; *$P \leq 0.05$; **$P \leq 0.01$; ***$P \leq 0.001$; ****$P \leq 0.0001$) in GraphPad Prism. Error bars represent one standard deviation. (D) Quantification of fluorescent puncta formed in HEK293T biosensor cells seeded with AD brain-extracted fibrils from AD1. Prior to seeding, fibrils were incubated with no treatment, vehicle (1% DMSO), EGCG, CNS-11, or one of the four chemical analogs of CNS-11. Final concentration of small molecule on biosensor cells was 12.5 μM. Statistical analysis was performed using one-way ANOVA followed by Tukey's multiple comparison test (ns, $P > 0.05$; *$P \leq 0.05$; **$P \leq 0.01$; ***$P \leq 0.001$; ****$P \leq 0.0001$) in GraphPad Prism. Error bars represent one standard deviation.

formation of additional fibrils might halt the progression of AD.

The small-molecule EGCG, abundant in green tea, has long been known to disaggregate amyloid fibrils.[24−26] However, EGCG has poor bioavailability, fails to penetrate the brain, and is readily modified in the body.[27] In a prior study to understand how EGCG disaggregates stable amyloid fibrils, we applied cryo-electron microscopy to determine the atomic structure of a cryo-trapped complex of EGCG bound to AD brain-extracted tau.[28] Using the EGCG binding site as a pharmacophore, we computationally screened ∼60,000 drug-like compounds that have characteristics favoring blood−brain barrier (BBB) permeability (following the Lipinski rule of five, low polar surface area, etc.). With experimental validation, we discovered lead compound CNS-11, which prevents seeding in a tau aggregation cell culture model and disaggregates AD patient brain-extracted tau fibrils in vitro.[28]

In this study, we screen four chemical analogs of CNS-11 for their ability to disaggregate AD patient brain-extracted tau fibrils in vitro. We identify two additional lead compounds, CNS-11D and CNS-11G, and determine that administration of

https://doi.org/10.1021/acschemneuro.5c00940
ACS Chem. Neurosci. XXXX, XXX, XXX−XXX

CNS-11D or CNS-11G reduces levels of insoluble tau in a mouse model of tauopathy.

RESULTS

Chemical Analogs of CNS-11 Disaggregate Tau Fibrils from AD Patients

We recently designed ten chemical analogs of a compound that disaggregates AD tau, CNS-11.[29] In preliminary in vitro experiments, four of these analogs showed a higher degree of promise for disaggregating AD brain-extracted tau fibrils compared to the other six analogs (data not shown). Therefore, we sought to determine whether four of the ten chemical analogs, CNS-11A, CNS-11B, CNS-11D, and CNS-11G (Figure 1A), can disaggregate tau fibrils extracted from post-mortem brain tissue of AD patients.

We extracted fibrils from post-mortem brain tissue of three AD patients (AD1, AD2, and AD3, Table S1). We incubated the AD brain-extracted fibrils with vehicle (1% DMSO), EGCG, CNS-11, or one of the four chemical analogs of CNS-11 and counted the fibrils visible by negative-staining electron microscopy. We then divided the fibril counts by counts of the vehicle-treated control to obtain a normalized fibril count. Incubation of AD1 with EGCG resulted in the greatest reduction of the number of AD brain-extracted fibrils compared with no treatment (normalized fibril count of 0.244). EGCG was followed by CNS-11D, CNS-11, CNS-11B, and CNS-11G (normalized fibril counts of 0.424, 0.459, 0.560, and 0.802, respectively, Figure 1B,C). Incubation of AD1 with neither vehicle nor CNS-11A reduced the number of AD brain-extracted fibrils compared with no treatment (normalized fibril counts of 1.048 and 0.943, respectively, Figure 1B,C). We observed similar findings with incubation of AD2 and AD3 with the same compounds (Figure S1).

Chemical Analogs of CNS-11 Prevent Seeding by Tau Fibrils from AD Patients in HEK293 Biosensor Cells

Next, we determined whether these chemical analogs prevent seeding by AD tau fibrils in a tau aggregation cell model. HEK293T biosensor cells stably express YFP-fused tau-K18.[17] When HEK293T biosensor cells are seeded by exogenous tau fibrils, endogenous YFP-fused tau-K18 aggregates and forms fluorescent, quantifiable puncta. We incubated AD brain-extracted fibrils from patient AD1 with vehicle (1% DMSO), EGCG, CNS-11, or one of the four chemical analogs of CNS-11 and seeded biosensor cells with the mixtures. Incubation with EGCG resulted in the greatest reduction of seeding by AD brain-extracted fibrils compared to no treatment (normalized puncta count of 0.020, Figure 1D). EGCG was followed by CNS-11G, CNS-11D, CNS-11, and CNS-11A (normalized puncta counts of 0.267, 0.349, 0.357, and 0.359, respectively; Figure 1D). Incubation with vehicle or CNS-11B did not reduce seeding by AD brain-extracted fibrils compared to no treatment (normalized puncta counts of 1.037 and 0.737, respectively; Figure 1D).

CNS-11 and CNS-11G Disaggregate Tau Fibrils from AD Patients at Concentrations Lower than 500 μM

Among the four chemical analogs, CNS-11D and CNS-11G showed the greatest promise as tau disaggregators because they were able to both reduce the number of AD brain-extracted fibrils and reduce seeding by AD tau fibrils in biosensor cells. We incubated AD brain-extracted fibrils from patient AD3 with vehicle (1% DMSO), CNS-11, CNS-11D, or CNS-11G at 25 and 100 μM and counted the fibrils visible by electron microscopy. Both CNS-11 and CNS-11G reduced the number of AD brain-extracted fibrils at 100 μM, and CNS-11G reduced the number of AD brain-extracted fibrils at 25 μM (Figure S2).

CNS-11, CNS-11D, and CNS-11G Prevent Seeding by Tau Fibrils at Dose below Their Respective LD50s

Next, we assessed the toxicity of CNS-11, CNS-11D, and CNS-11G on cultured Neuro-2a (N2a) neuronal cells using a 3-(4,5-dimethylthiazol-2-yl)-2,5-diphenyltetrazolium bromide (MTT) dye reduction cell viability assay. The LD50s of CNS-11, CNS-11D, and CNS-11G were 5.5 μM, 27.6 μM, and 20.4 μM, respectively (Figure S3). We incubated AD brain-extracted fibrils from patient AD1 with vehicle (1% DMSO), CNS-11, CNS-11D, or CNS-11G at various concentrations and seeded biosensor cells with the mixtures. CNS-11, CNS-11D, or CNS-11G reduces seeding by AD tau fibrils in biosensor cells in a dose-dependent manner (Figure S4). It was not possible to determine IC_{50}s of the small molecules as we were unable to obtain measurements of seeding inhibition at doses higher than 5 μM due to their poor solubility. However, CNS-11 reduced seeding by 45% compared to the vehicle-treated control at 2.5 μM, CNS-11D reduced seeding by 50% compared to the vehicle-treated control, and CNS-11G reduced seeding by 54% compared to the vehicle-treated control. CNS-11, CNS-11D, and CNS-11G all reduced seeding by approximately 50% at doses lower than their respective LD50s.

CNS-11, CNS-11D, and CNS-11G Prevent Seeding by Fibrils from Multiple Tauopathies in HEK293 Biosensor Cells

Next, we determined whether these chemical analogs prevent seeding by fibrils from other tauopathies in HEK293T biosensor cells. We extracted fibrils from post-mortem brains of patients with AD, Pick's disease (PiD), corticobasal degeneration (CBD), or progressive supranuclear palsy (PSP). We incubated the brain-extracted fibrils as well as recombinant tau-K18+ fibrils with vehicle (1% DMSO), CNS-11, CNS-11D, and CNS-11G and seeded biosensor cells with the mixtures.

Incubation with CNS-11 resulted in reduction of seeding by AD brain-extracted fibrils (normalized puncta count of 0.832) and PiD fibrils (normalized puncta count of 0.646) compared to no treatment but not CBD, PSP, or K18+ fibrils (Figure S5A). Incubation with CNS-11D resulted in reduction of seeding by AD brain-extracted fibrils (normalized puncta count of 0.837) and K18+ fibrils (normalized puncta count of 0.645) compared to no treatment but not PiD, CBD, or PSP fibrils (Figure S5B). Incubation with CNS-11G resulted in reduction of seeding by AD brain-extracted fibrils (normalized puncta count of 0.551) and K18+ fibrils (normalized puncta count of 0.163) compared to no treatment but not PiD, CBD, or PSP fibrils (Figure S5C). CNS-11, CNS-11D, and CNS-11G each halted seeding by tau fibrils from multiple sources.

CNS-11, CNS-11D, and CNS-11G Do Not Inhibit Primary Tau Aggregation

To assess whether CNS-11, CNS-11D, or CNS-11G influences primary tau aggregation, we performed a ThT aggregation kinetics assay (Figure S6). No difference is seen in lag time and maximum ThT intensity between recombinant tau-K18+ allowed to aggregate in the presence of either CNS-11, CNS-11D, or CNS-11G compared to vehicle under the conditions tested.

https://doi.org/10.1021/acschemneuro.5c00940
ACS Chem. Neurosci. XXXX, XXX, XXX−XXX

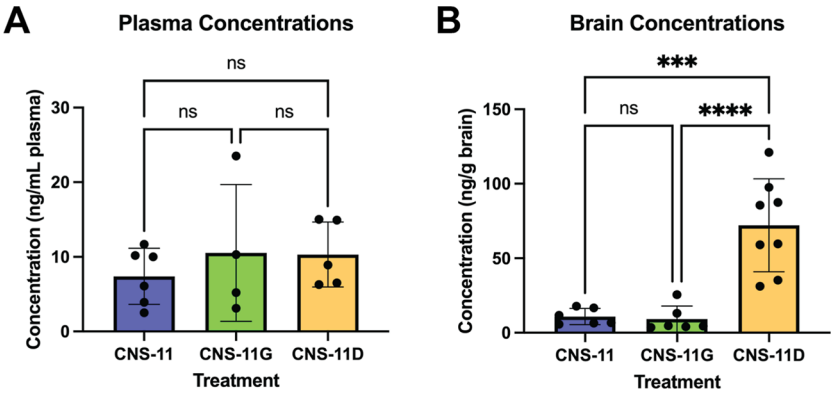

Figure 2. Brain penetration of CNS-11D in mice. (A,B) Mice were injected intravenously with 1 mg/kg CNS-11D (n = 8) and euthanized 1 h after dosing. Compound levels in (A) plasma and (B) brain tissue were analyzed using an LC−MS/MS-MRM method. Statistical analysis was performed using two-way ANOVA (multiple comparisons using Šídák's multiple comparisons test; ns, $p > 0.05$; *, $p < 0.05$; **, $p < 0.01$; ***, $p < 0.001$; ****, $p < 0.0001$) in GraphPad Prism. Error bars represent one standard deviation. Note: n = 5 for plasma because the amount of plasma collected from three of eight mice treated with CNS-11D was an insufficient volume for analysis by LC−MS/MS-MRM.

CNS-11D and CNS-11G Are Soluble under Physiological Conditions

Before moving to in vivo testing, we determined the water solubilities of CNS-11, CNS-11D, and CNS-11G. We mixed them with deuterated water and measured their concentrations using nuclear magnetic resonance spectroscopy. We determined the water solubilities of CNS-11D and CNS-11G to be 17.5 μM and 40 μM, respectively (Table S2, Figure S7). The water solubility of CNS-11 was below the limit of detection (<1 μM).

CNS-11D Crosses the Mouse BBB More Readily than CNS-11 and CNS-11G

Because CNS-11D and CNS-11G showed promise as tau disaggregators, we next assessed their ability to cross the mouse BBB. We previously determined that CNS-11 and CNS-11G penetrate the brain.[29] CNS-11 was measured in mouse brain tissue with a range of concentrations of 5.7−17.8 ng/g brain, and CNS-11G was measured in brain tissue with a range of concentrations of 3.5−25.5 ng/g brain. Following the same protocol, we administered CNS-11D by tail vein injection at a dose of 1 mg/kg to wild-type B6C3F1/J mice (n = 8 for each compound). 1 h after dosing, we euthanized the mice by cardiac perfusion and collected brain and plasma samples. A liquid chromatographic−tandem mass spectrometric multiple reaction monitoring (LC−MS/MS-MRM) assay was used to detect and quantify the drug levels in each tissue sample. The sample extraction protocol for the plasma and brain was optimized with spiking experiments in which the authentic compounds were added to the plasma and brain from drug-naive mice.[29]

One hour following administration, CNS-11D was measured in the plasma of treated wild-type mice with a range of concentrations of 6.3−15.0 ng/mL (Figure 2A). CNS-11D was measured in brain tissue with a range of concentrations of 31.2−121.1 ng/g brain (Figure 2B). Plasma levels of CNS-11D were not different from those measured for CNS-11 and CNS-11G, but brain levels of CNS-11D were five to seven times higher than those measured for CNS-11 and four to eight times higher than those measured for CNS-11G (Figure 2A,B).

CNS-11 Reduces Levels of Insoluble Tau in Unilaterally Seeded PS19 Mice

We first characterized CNS-11 in the PS19 mouse model of tauopathy to determine whether CNS-11 causes toxicity and to pilot study its effect on tau aggregation in vivo. PS19 mice express human tau with the pathogenic pro-aggregation P301S mutation and develop hyperphosphorylated tau inclusions after six months of age.[30] Young PS19 mice can be seeded by intracranial injection of tau fibrils to rapidly induce tau pathology and to ensure consistency in tau spreading among mice.[20] We stereotaxically seeded 10 two-month-old PS19 mice with tau-K18+ preformed fibrils in the right hippocampus and the right frontal cortex, as previously described.[31] In addition, we stereotaxically injected PBS in 4 wild-type, age-matched B6C3F1/J mice to serve as controls. Beginning 4 weeks after surgery, we administered CNS-11 at a dose of 1 mg per kg of body weight (mg/kg) by tail vein injection to n = 5 PS19 mice and vehicle (1× PBS with 10% DMSO) to n = 5 PS19 mice, once a week for 8 weeks. We measured their weight before each administration (Figure 3A).

After 8 weeks of treatment, we assessed the wild-type and PS19 mice using the Barnes maze, a test for spatial memory in which PS19 mice have previously demonstrated a deficit.[32] The mice were introduced to a table with multiple holes, and they learned to find the location of the "escape" hole over the course of multiple days (Figure S8A). On the final day, we removed the escape hole and assessed how quickly they went to the location of the former escape hole (Figure S8B) and how many times they returned to that location (Figure S8C). We observed large variations among mice in each group due to a small cohort and therefore did not find a statistically significant deficit in the PS19 mice compared to wild-type mice or a statistically significant difference in PS19 mice treated with CNS-11 compared to the vehicle.

After behavior testing, we euthanized the mice by cardiac perfusion and collected brain tissue. We homogenized the right hippocampi in RIPA buffer, separated the homogenate into RIPA-soluble and RIPA-insoluble fractions, and performed a Western blot analysis of both fractions. Seeded PS19 mice had higher levels of soluble tau and insoluble tau compared to wild-type mice (1.202 normalized intensity vs 0.4662 normalized intensity for soluble tau, 0.9733 normalized intensity vs 0.4147 normalized intensity for insoluble tau, Figures 3B−D, S9).

https://doi.org/10.1021/acschemneuro.5c00940
ACS Chem. Neurosci. XXXX, XXX, XXX−XXX

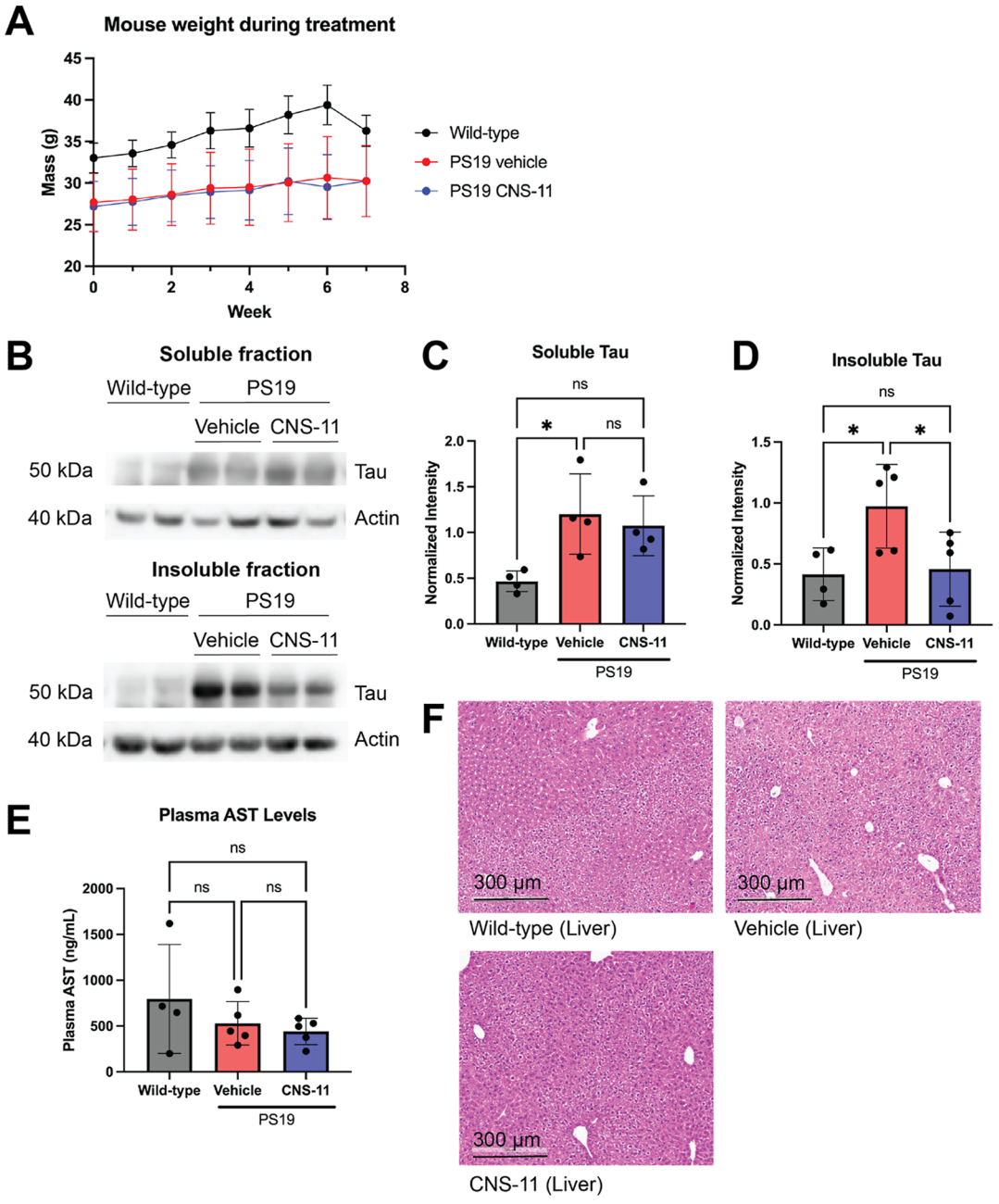

Figure 3. CNS-11 reduces levels of insoluble tau in PS19 mice without causing obvious toxicity. (A) CNS-11 at a dose of 1 mg per kg of body weight (mg/kg) was administered by tail vein injection to $n = 5$ mice, and vehicle (1× PBS with 10% DMSO) was administered to $n = 5$ mice, once a week for 8 weeks. The weight of each mouse was recorded weekly. (B) The right hippocampus of each mouse was homogenized in RIPA buffer, separated into RIPA-soluble and RIPA-insoluble fractions, and analyzed by Western blot analysis with an antitau antibody (Dako). (C) Seeded PS19 mice had significantly higher levels of soluble tau compared to wild-type mice. Treatment of PS19 mice with CNS-11 did not significantly change levels of tau in the soluble fraction. Statistical analysis was performed using two-way ANOVA (multiple comparisons using Šídák's multiple comparisons test; ns, $p > 0.05$; *, $p < 0.05$; **, $p < 0.01$; ***, $p < 0.001$; ****, $p < 0.0001$) in GraphPad Prism. Error bars represent one standard deviation. (D) Seeded PS19 mice had significantly higher levels of in soluble tau compared to wild-type mice. Treatment of PS19 mice with CNS-11 significantly reduced levels of tau in the insoluble fraction. Statistical analysis was performed using two-way ANOVA (multiple comparisons using Šídák's multiple comparisons test; ns, $p > 0.05$; *, $p < 0.05$; **, $p < 0.01$; ***, $p < 0.001$; ****, $p < 0.0001$) in GraphPad Prism. Error bars represent one standard deviation. (E) Treatment with CNS-11 did not significantly change plasma AST levels, indicating that it does not affect liver function. Statistical analysis was performed using two-way ANOVA (multiple comparisons using Šídák's multiple comparisons test; ns, $p > 0.05$; *, $p < 0.05$; **, $p < 0.01$; ***, $p < 0.001$; ****, $p < 0.0001$) in GraphPad Prism. Error bars represent one standard deviation. (F) H&E-stained tissue sections from the liver of wild-type or PS19 mice treated with vehicle or CNS-11. Degenerative changes limited to periductal hepatocytes are visible in the livers of wild-type mice. Degenerative changes extending from periductal hepatocytes to the centrilobular region are visible in the livers of PS19 mice treated with vehicle, and degenerative changes limited to periductal hepatocytes are visible in the livers of PS19 mice treated with CNS-11.

Treatment of PS19 mice with CNS-11 did not change levels of tau in the soluble fraction compared to treatment with vehicle (1.074 normalized intensity vs 1.202 normalized intensity, Figures 3B,C, S9). However, treatment with CNS-11 reduced

https://doi.org/10.1021/acschemneuro.5c00940
ACS Chem. Neurosci. XXXX, XXX, XXX−XXX

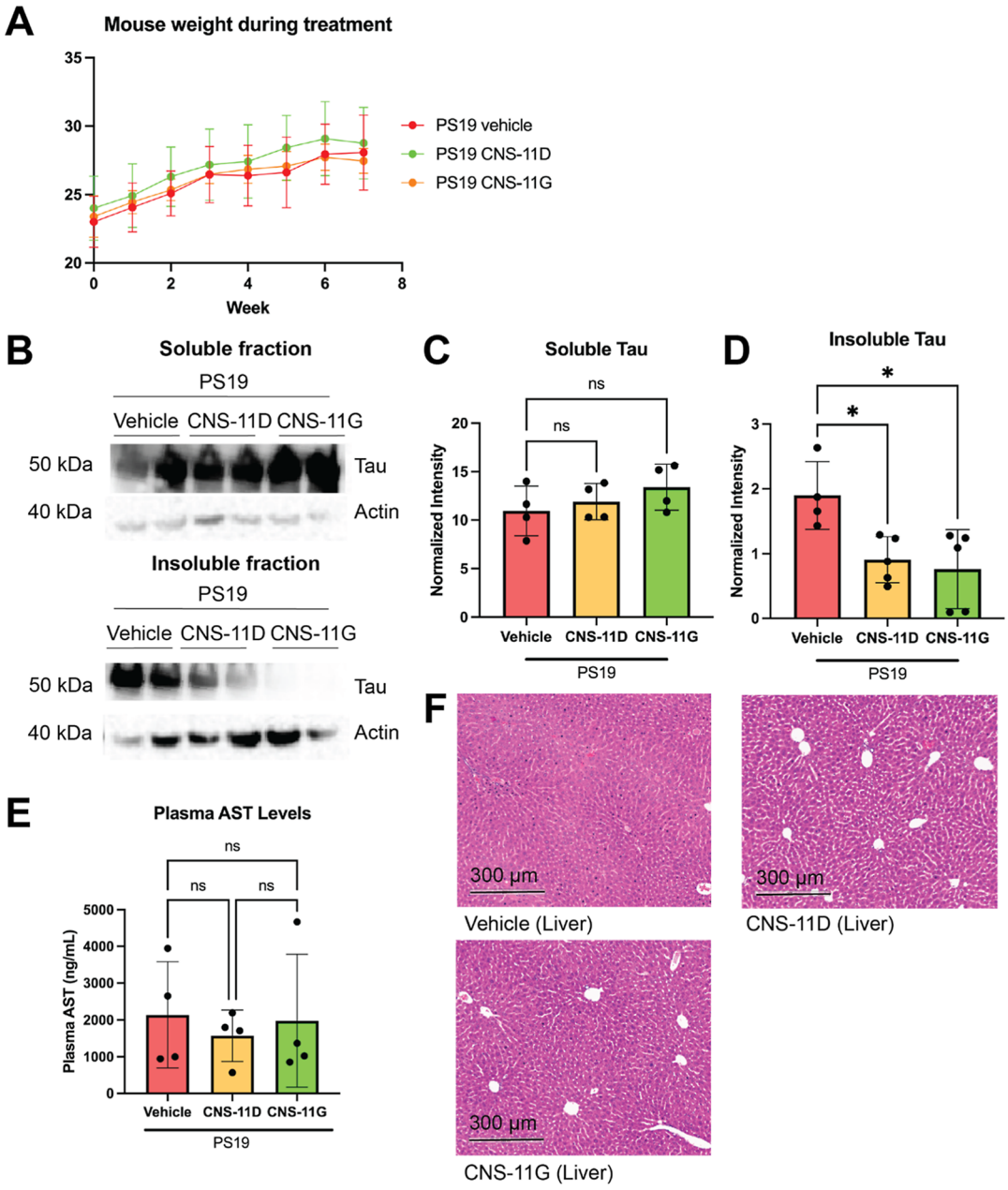

Figure 4. CNS-11D and CNS-11G both reduce levels of insoluble tau in PS19 mice without causing obvious toxicity. (A) CNS-11D or CNS-11G at a dose of 1 mg per kg of body weight (mg/kg) was administered by tail vein injection to $n = 5$ mice, and vehicle (1× PBS with 10% DMSO) was administered to $n = 5$ mice, once a week for 8 weeks. The weight of each mouse was recorded weekly. (B) The right hippocampus of each mouse was homogenized in RIPA buffer, separated into RIPA-soluble and RIPA-insoluble fractions, and analyzed by Western blot analysis with an antitau antibody (Dako). (C) Treatment of PS19 mice with CNS-11D or CNS-11G did not significantly change levels of tau in the soluble fraction. Statistical analysis was performed using two-way ANOVA (multiple comparisons using Šídák's multiple comparisons test; ns, $p > 0.05$; *, $p < 0.05$; **, $p < 0.01$; ***, $p < 0.001$; ****, $p < 0.0001$) in GraphPad Prism. Error bars represent one standard deviation. (D) Treatment of PS19 mice with either CNS-11D or CNS-11G significantly reduced levels of tau in the insoluble fraction. Statistical analysis was performed using two-way ANOVA (multiple comparisons using Šídák's multiple comparisons test; ns, $p > 0.05$; *, $p < 0.05$; **, $p < 0.01$; ***, $p < 0.001$; ****, $p < 0.0001$) in GraphPad Prism. Error bars represent one standard deviation. (E) Treatment with CNS-11D or CNS-11G did not significantly change plasma AST levels, indicating that they do not affect liver function. Statistical analysis was performed using two-way ANOVA (multiple comparisons using Šídák's multiple comparisons test; ns, $p > 0.05$; *, $p < 0.05$; **, $p < 0.01$; ***, $p < 0.001$; ****, $p < 0.0001$) in GraphPad Prism. Error bars represent one standard deviation. (F) H&E-stained tissue sections from the liver of PS19 mice treated with vehicle, CNS-11D, or CNS-11G. Dark discoloration in scattered nuclei is visible in the livers of PS19 mice treated with vehicle, and dark discoloration in rare nuclei and mild distention of sinusoid is visible in the livers of PS19 mice treated with CNS-11D or CNS-11G. There are no signs of liver injury in any group.

levels of tau in the insoluble fraction compared to treatment with vehicle (0.4570 normalized intensity vs 0.9733 normalized intensity, Figures 3B,D, S9).

CNS-11 Does Not Cause Obvious Toxicity in PS19 Mice after 8 Weeks of Treatment

Additionally, we collected plasma and major organs, including the heart, lung, kidney, liver, and spleen. We measured plasma

https://doi.org/10.1021/acschemneuro.5c00940
ACS Chem. Neurosci. XXXX, XXX, XXX−XXX

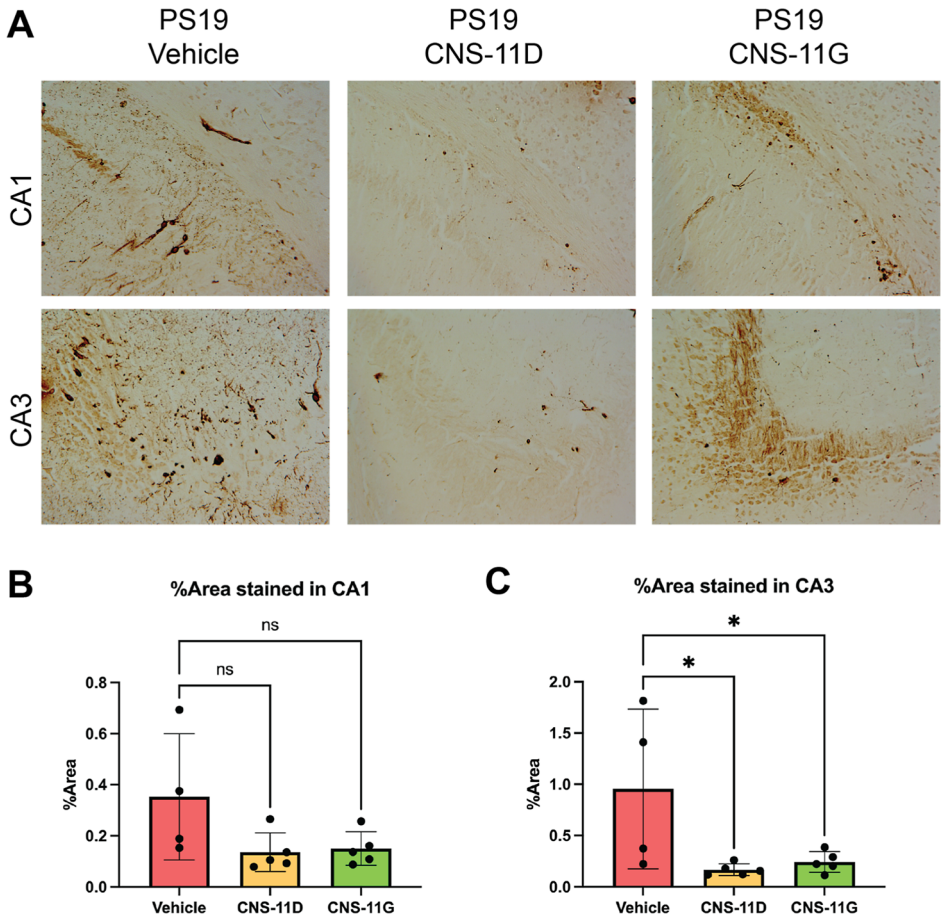

Figure 5. CNS-11D and CNS-11G both reduce phosphorylated tau in the hippocampus of PS19 mice. (A) Representative immunohistochemical images of CA1 and CA3 in the left hippocampus of PS19 mice treated with vehicle, CNS-11D, or CNS-11G. Tissue was stained with AT8 antibody for phosphorylated tau at residues Ser202/Thr205 and imaged at 10× magnification. (B,C) Percentage of area stained in (B) CA1 and (C) CA3 was quantified using ImageJ. Statistical analysis was performed using one-way ANOVA followed by Tukey's multiple comparison test (ns, $P > 0.05$; *$P \leq 0.05$; **$P \leq 0.01$; ***$P \leq 0.001$; ****$P \leq 0.0001$) in GraphPad Prism. Error bars represent one standard deviation.

aspartate aminotransferase (AST) levels to assess the liver function. Treatment with CNS-11 did not change plasma AST levels, indicating that it does not grossly affect liver function (Figure 3E). We performed hematoxylin and eosin (H&E) staining on sections of the liver, heart, lung, spleen, and kidney. In the livers of wild-type mice treated with the vehicle, we observed degenerative changes limited to periductal hepatocytes (Figure 3F). In the livers of PS19 mice treated with the vehicle, we observed degenerative changes extending from periductal hepatocytes to the centrilobular region, whereas in the livers of PS19 mice treated with CNS-11, we observed degenerative changes limited to periductal hepatocytes (Figure 3F). These findings indicate that treatment with CNS-11 does not cause obvious toxicity to the liver beyond that of the vehicle. We did not observe any degenerative changes in the heart, lung, spleen, or kidney of wild-type mice or PS19 mice treated with vehicle or CNS-11 (Figure S10). In addition, treatment with CNS-11 did not significantly lower body weight compared with treatment with vehicle (Figure 3A). Together, these findings indicate that treatment with CNS-11 at 1 mg/kg, a dose that reduces levels of insoluble tau, does not cause obvious toxicity to PS19 mice.

Tau Pathology in Unilaterally Seeded PS19 Mice Is Insufficient to Determine Effects of CNS-11

Finally, we fixed the left cerebral hemispheres, contralateral to seeding, from the PS19 mice treated with vehicle or CNS-11. We sectioned the tissue into 10 μm thick sections and stained sections from the hippocampus with AT8 antibody for phosphorylated tau at residues Ser202/Thr205. However, there was insufficient pathological change for analysis on the left hemisphere as the PS19 mice were seeded in the right hippocampus and the right frontal cortex. Because we were unable to obtain tissue suitable for analysis, we cannot conclude that CNS-11 reduces tau pathology in PS19 mice.

CNS-11D and CNS-11G Each Reduce Levels of Insoluble Tau in Bilaterally Seeded PS19 Mice

After demonstrating that CNS-11 does not cause obvious toxicity in PS19 mice, we sought to determine whether CNS-11G and CNS-11D can halt tau aggregation in seeded PS19 mice. To ensure the development of sufficient tau pathology in both hemispheres of the brain, we stereotaxically seeded 15 two-month-old PS19 mice with tau-K18+ preformed fibrils in the left hippocampus and the right hippocampus. Beginning 2 weeks after surgery, we administered CNS-11G or CNS-11D at a dose of 1 mg/kg by tail vein injection to $n = 5$ mice and vehicle (1× PBS with 10% DMSO) to $n = 5$ mice, once a week for 8 weeks. We measured their weight before each

https://doi.org/10.1021/acschemneuro.5c00940
ACS Chem. Neurosci. XXXX, XXX, XXX−XXX

administration (Figure 4A). One mouse in the vehicle group was lost during the sixth week of treatment due to health concerns unrelated to the study.

After 8 weeks of treatment, we euthanized the mice by cardiac perfusion and collected brain tissue. We homogenized the right hippocampi in RIPA buffer, separated the homogenate into RIPA-soluble and RIPA-insoluble fractions, and performed Western blot analysis of both fractions. Treatment of PS19 mice with CNS-11D did not change levels of tau in the soluble fraction compared to treatment with vehicle (11.91 normalized intensity vs 10.96 normalized intensity, Figures 4B,C, S11). However, treatment with CNS-11D reduced levels of tau in the insoluble fraction compared to treatment with vehicle (0.9057 normalized intensity vs 1.898 normalized intensity, Figures 4B,D, S11). Treatment of PS19 mice with CNS-11G did not change levels of tau in the soluble fraction compared to treatment with vehicle (13.39 normalized intensity vs 10.96 normalized intensity, Figures 4B,C, S11). However, treatment with CNS-11G reduced levels of tau in the insoluble fraction compared to treatment with vehicle (0.7619 normalized intensity vs 1.898 normalized intensity, Figures 4B,D, S11).

CNS-11D and CNS-11 Do Not Cause Obvious Toxicity in PS19 Mice after 8 Weeks of Treatment

Additionally, we collected plasma and major organs, including heart, lung, kidney, liver, and spleen. We measured plasma AST levels to assess the liver function. Treatment with either CNS-11D or CNS-11G did not change plasma AST levels, indicating that they do not affect liver function (Figure 4E). We performed hematoxylin and eosin (H&E) staining on sections of the liver, heart, lung, spleen, and kidney. In the livers of PS19 mice treated with the vehicle, we observed dark discoloration in scattered nuclei, and in the livers of PS19 mice treated with CNS-11D or CNS-11G, we observed dark discoloration in rare nuclei and mild distention of sinusoids (Figure 4F). However, we did not observe signs of liver injury in any group, indicating that treatment with CNS-11D or CNS-11G does not cause obvious toxicity to the liver beyond that of the vehicle. We did not observe any degenerative changes in the heart, lung, spleen, or kidney of wild-type or PS19 mice treated with vehicle or CNS-11D or CNS-11G (Figure S12). In addition, treatment with CNS-11D or CNS-11G did not significantly lower body weight compared to treatment with vehicle (Figure 4A). Together, these findings indicate that CNS-11D and CNS-11G do not cause obvious toxicity to PS19 mice at a dose that can reduce levels of insoluble tau in vivo.

CNS-11D and CNS-11G Each Reduces Tau Pathology in Bilaterally Seeded PS19 Mice

Finally, we fixed the left cerebral hemispheres from the PS19 mice treated with vehicle, CNS-11D, or CNS-11G. We sectioned the tissue into 10 μm thick sections and stained sections from the hippocampus with AT8 antibody for phosphorylated tau at residues Ser202/Thr205 (Figures 5A, S13). We imaged at 10× magnification and quantified the percentage of area stained in CA1 and CA3 of the hippocampus in each mouse. Treatment of PS19 mice with CNS-11D did not reduce the percentage of area stained in CA1 of the hippocampus compared to treatment with vehicle (0.1360% area compared to 0.3530% area, Figure 5B). However, CNS-11D did reduce the percentage of area stained in CA3 of the hippocampus compared to treatment with vehicle (0.1674% area compared to 0.9553% area, Figure 5C). Treatment of PS19 mice with CNS-11G did not reduce the percentage of area stained in CA1 of the hippocampus compared to treatment with vehicle (0.1504% area compared to 0.3530% area, Figure 5B). However, CNS-11G did reduce the percentage of area stained in CA3 of the hippocampus compared to treatment with vehicle (0.2432% area compared to 0.9553% area, Figure 5C). Altogether, these results demonstrate that CNS-11D and CNS-11G reduce tau pathology in PS19 mice without causing obvious toxicity.

DISCUSSION

Tau aggregation in patients is correlated with brain atrophy and cognitive decline,[3−6] so it is a promising therapeutic target. Currently, 32 tau-targeting therapeutics are in clinical trials.[33] Of those 32 therapeutics, 18 are immunotherapies, and 12 are small-molecule therapies. Most of these are in the early stages of clinical trials, with the exception of one Phase 2/3 trial of ACI-35, a vaccine that elicits an antibody response to tau,[34] and multiple phase 3 trials of HMTM, a small molecule that inhibits tau aggregation.[35−39] Tau-targeting immunotherapies have failed or have so far shown only modest slowing of disease progression in clinical trials. The current therapeutics approved by the FDA need to be administered intravenously biweekly at specialized infusion centers, and are very costly.[1,40,41] Therefore, there is a need to explore small-molecule compounds as an alternative avenue to treat AD. Small-molecule compounds are generally orally available, increasing patient compliance and reducing manufacture cost. Small molecules are also less likely to trigger autoimmune response which can lead to adverse side effects.[42] Because of these advantages, small molecules targeting all aspects of tau pathology, from truncation to oligomerization, are being pursued.[43,44] We decided to focus on small-molecule tau-targeting therapeutics that disaggregate already formed fibers.

Our class of small-molecule disaggregators provides a different avenue of disease intervention compared to previous small-molecule tau-targeting therapeutics, which are largely tau aggregation inhibitors. HMTM, the only tau therapeutic that has entered phase 3 trials, is a second-generation formulation of methylene blue. HMTM, like methylene blue, has been shown to inhibit recombinant tau fibrils,[45,46] and therefore has been the frontrunner inhibitor of tau fibrils. However, HMTM has demonstrated limited efficacy in Phase 3 clinical trials,[35,36] despite great bioavailability and behavioral rescue in multiple mouse models.[47] Despite these findings, HMTM is still believed to have potential, as new research continues to dissect its modes of action[39,48] and push for more rigorous clinical trials. In parallel, we decided to explore tau fibril disaggregators instead of inhibitors. By directly isolating AD tau fibrils, we directly observed the disaggregation of our target ex vivo model. Then, we observed a corresponding disaggregation in a mouse model by measuring a decrease in insoluble tau content, which is one aspect the current tau inhibitor drugs are lacking.[47] By discovering tau fibril disaggregators as a complement to the promising current research on tau fibril inhibitors, we can remove and prevent tau aggregation at multiple stages and potentially extend the therapeutic window from patients with mild cognitive impairment to those further along in disease progression.

As previously described, CNS-11 emerged as an AD tau fibril disaggregator in a pharmacophore guided screen based on our structure of a pan-amyloid disaggregator, EGCG

https://doi.org/10.1021/acschemneuro.5c00940
ACS Chem. Neurosci. XXXX, XXX, XXX−XXX

complexed with tau PHF.[28] In the present study, we applied a rigorous experimental procedure to identify additional tau fibril disaggregators using ex vivo brain materials from human patients. We screened four chemical analogs related to known disaggregator CNS-11 and found three, CNS-11B, CNS-11D, and CNS-11G, that reduced the number of AD brain-extracted fibrils quantifiable by EM (Figure 1B,C). Because tau aggregates spread across the brain through *trans*-synaptic seeding,[18] it is crucial for the products of amyloid disaggregation to lack seeding ability.[49] Therefore, we verified that our disaggregators do not produce toxic, seed-competent, soluble tau species by testing the seeding ability of disaggregated products using the biosensor cell assay. Of the chemical analogs of CNS-11, only CNS-11D and CNS-11G reduce seeding in a tau aggregation cell culture model (Figure 1D). On further study, CNS-11, CNS-11D, and CNS-11G each reduce seeding in biosensor cells in a dose-dependent manner and do so at doses lower than that of their LD_{50} in N2a cells (Figure S3).

Aggregation of tau is a histological hallmark of AD and other, rarer neurodegenerative diseases, including PiD, CBD, and PSP. Recent studies have shown that tau fibrils from each disease have distinct atomic structures.[52] Furthermore, almost all of the widely used recombinant tau constructs and mouse models produce fibrils with different atomic structures.[53,54] Therefore, we assessed whether CNS-11, CNS-11D, and CNS-11G halt seeding by tau fibrils with different structures from post-mortem brain extract of patients with PiD, CBD, and PSP, as well as recombinant tau-K18+ fibrils. CNS-11 halts seeding from AD and PiD fibrils (Figure S5A), and CNS-11D and CNS-11G each halt seeding from AD and recombinant tau-K18+ fibrils (Figure S5B,C). In a previous study, we screened CNS-11 and the ten chemical analogs for their ability to disaggregate recombinant and patient derived α-synuclein fibrils. We discovered that both CNS-11 and one of its analogs, CNS-11G, disaggregate recombinant α-synuclein fibrils and multiple system atrophy patient brain-extracted fibrils and prevent seeding in an α-synuclein aggregation cell culture model.[29] Combined with results from the previous study, the results of this study demonstrate CNS-11, CNS-11D, and CNS-11G behave as multiamyloid disaggregators, with effects on both tau and α-synuclein fibrils with different structures.

We also report the water solubility of CNS-11, CNS-11D, and CNS-11G. CNS-11D and CNS-11G are soluble under physiological aqueous conditions in the micromolar range, while CNS-11 has a solubility below the limit of detection (Figure S7). The limited solubility of all three compounds is not surprising as these compounds all have physiochemical properties that favor BBB penetrance. Compounds need to be sufficiently lipophilic to cross the BBB,[50,51] and we demonstrated our compounds are brain penetrant. However, we acknowledge that poor water solubility limits in vivo and cell testing as these experiments largely take place in an aqueous setting. We plan to improve the solubility of our lead compounds CNS-11D and CNS-11G through functional group modification and addition of counterions.

Next, we assessed the brain penetrance of CNS-11, CNS-11D, and CNS-11G. Compounds in the CNS-drug set are predicted to have physiochemical properties that favor entrance into the central nervous system through the BBB.[55] We found that brain levels of CNS-11D after one-time treatment were higher than those previously reported for CNS-11 or CNS-11G[29] (Figure 2). Therefore, we administered CNS-11D and CNS-11G weekly in PS19 mice for 8 weeks to assess whether these compounds have an effect on tau disaggregation. We found that 8 weeks of treatment with either CNS-11D or CNS-11G reduced levels of insoluble tau in the PS19 mouse model of tauopathy (Figure 4B−D). Interestingly, we did not observe a corresponding increase in the levels of tau in the soluble fraction (Figure 4C). It is possible that baseline levels of soluble tau are too high in PS19 mice to observe any meaningful changes in the soluble fraction. Furthermore, disaggregated tau may not simply be solubilized by the CNS compounds but instead quickly turned over or degraded by the lysosomal pathway or other clearance mechanisms. In addition, we visualized reductions in the CA3 region of AT8-stained brain sections from mice treated with CNS-11D or CNS-11G (Figure 5A−C). We did not observe a reduction in tau pathology in the CA1 region (Figure 5B), possibly because the CA1 region has a lower amount of tau pathology than CA3, and our sample size was too small to observe a statistically significant change. Finally, we observed that CNS-11, CNS-11D, and CNS-11G do not cause obvious toxicity in PS19 mice (Figures 4E,F, S12), demonstrating that CNS-11D and CNS-11G can reduce tau aggregation at a concentration not toxic to mice.

CNS-11D and CNS-11G reduced tau aggregation in PS19 mice, although single-dose concentrations were lower than the therapeutic window of the micromolar range that we discovered ex vivo. There are several reasons that could account for the discrepancy. The AD-extracted fibrils that we used are concentrated during the extraction process (equivalent to 500 nM of tau-K18+), and the physiologic concentration of tau fibrils is lower in mouse brain. In addition, the water solubilities of these compounds as measured by NMR are relatively poor. Therefore, the concentration of small molecules we reported for the ex vivo and in cell experiments could be overestimated, as we assume complete solubility when calculating the concentrations of small molecules. Second, we measured brain levels only after single-dose administration, and CNS-11D and CNS-11G, which are highly lipophilic, could have accumulated in the brains of PS19 mice. Brain levels of CNS-11D after one-time treatment were significantly higher than those previously reported for CNS-11G, but the two molecules exerted similar effects after 8 weeks of treatment, which supports the hypothesis that these molecules accumulate in the brain over time. Finally, in ex vivo experiments, AD-extracted fibrils were only treated for 24 h, whereas the time the small molecules remain in the brains of PS19 mice could be longer. These factors could account for the apparent discrepancy in efficient dose that we observed ex vivo and in vivo. Nonetheless, the decrease in insoluble pathology that we see in PS19 mice is still a promising sign of delayed or even reversed disease progression. Multiple animal models for tauopathies and other neurodegenerative diseases have linked amyloid pathologic change to other facets of disease, such as metabolism and general brain health.[56−58]

A limitation to our study is that experiments were performed on small groups of mice (n = 5 in each treatment group). Although these group sizes were large enough to show differences in levels of insoluble tau and phosphorylated tau pathology, they were not large enough to show statistically meaningful differences in behavior in the Barnes maze. Future studies with larger sample sizes are necessary to draw

https://doi.org/10.1021/acschemneuro.5c00940
ACS Chem. Neurosci. XXXX, XXX, XXX−XXX

conclusions about whether treatment with CNS-11, CNS-11D, or CNS-11G can improve memory deficits in PS19 mice.

AD-derived patient fibrils have been shown to have a very consistent PHF structure.[59] By using an ex vivo model, we directly measured the disaggregation of AD tau fibrils by our small-molecule candidates and identified candidates that have known disaggregation effects on the most relevant pathogenic species. Once disaggregation abilities were fully established in the ex vivo model, we progressed to assessing small-molecule disaggregator candidates in the widely used PS19 in vivo model. This study is the first in which we have extended our small-molecule disaggregation characterization from an ex vivo system to in vivo models. Overall, our work reveals two small molecules, CNS-11D and CNS-11G that disaggregate ex vivo AD tau fibrils, halt seeding in a cell culture model, and reduce levels of insoluble tau and reduce tau pathology in the brains of PS19 mice.

METHODS

Extraction of Tau Fibrils from Patient Brain Tissue

Human autopsy samples were obtained by the UCLA Pathology Department according to HHS regulations from patients consenting to autopsy. Samples were provided to the researchers in this study as anonymized tissues. For purification of fibrils from human post-mortem brain tissue, extractions were performed according to the previously published protocol[60] without performing size exclusion chromatography. The fibers are resuspended in 100 μL of 20 mM Tris-HCl at pH 7.4 containing 100 mM NaCl per gram of tissue.

Transmission EM/Negative Stain Grid Preparation and Fibril Counting

AD brain-extracted fibrils were incubated for 24 h at 37 °C with each small molecule (or vehicle) in 1× PBS at varying concentrations of small molecule and 500 nM of tau. Samples for TEM were prepared by applying 2 μL of the sample on glow-discharged 400 mesh carbon-coated Formvar support films mounted on copper grids (Ted Pella, Inc.). The samples were allowed to adhere for 1 min and then stained for 2 min with 4 μL of 2% uranyl acetate. The samples were then washed with another 4 μL of uranyl acetate and allowed to dry for 15 min. Each grid was inspected using a T12 (FEI) electron microscope. For each sample, three squares on the grid were randomly picked; and for each square, 18−26 micrographs were randomly taken at a magnification of 6,800×. So a total of 59−70 micrographs were recorded for each sample. Fibrils were counted manually using a cell counter.

Recombinant Tau-K18+ Expression and Purification

Recombinant tau-K18+ was expressed and purified as previously described.[61]

Biosensor Cell Seeding Assay

HEK293T cell lines stably expressing tau-K18 P301S-eYFP were obtained from Marc Diamond[17] and used without further characterization or authentication. Cells were maintained in DMEM (Life Technologies, cat. no. 11965092) supplemented with 10% (v/v) FBS (Life Technologies, cat. no. A3160401), 1% penicillin/streptomycin (Life Technologies, cat. 15140122), and 1% Glutamax (Life Technologies, cat. 35050061) at 37 °C, 5% CO_2 in a humidified incubator. Brain-extracted fibrils were incubated at 4 °C for 24 h in OptiMEM with each small molecule (or vehicle) at varying concentrations of small molecule and 500 nM of tau. For seeding, inhibitor-treated seeds were sonicated in a cup horn water bath for 5 min and then mixed with 1 volume of Lipofectamine 2000 (Life Technologies, cat.11668019) prepared by diluting 1 μL of Lipofectamine stock solution in 19 μL of OptiMEM. After 20 min, 10 μL of the mixture was added to 100 μL of tau biosensor cells, resulting in a final concentration of 12.5 μM of small molecule. The number of seeded aggregates was determined by imaging the entire well of a 96-well plate in triplicate using a Celigo Image Cytometer (Nexcelom) in the YFP channel. The number of aggregates in each image was determined using an ImageJ 2.3.050 script, which subtracts the background fluorescence from unseeded cells and then counts the number of aggregates as peaks with fluorescence above the background using the built-in particle analyzer. The number of aggregates was normalized to the confluence of each well, and dose−response plots were generated by calculating the average and standard deviations from triplicate measurements.

ThT Fluorescence Assay

Aliquots of purified, recombinant tau K18+ were thawed and diluted into PBS (pH 7.4) to a final concentration of 25 μM, in a solution with 40 μM ThT, 225 μg/mL heparin (H3393, Sigma-Aldrich), and 10 mM dithiothreitol (DTT) in a black Nunc 96-well optical bottom plate (Thermo Fisher Scientific). 10% DMSO (control), CNS-11, and its analogs CNS-11D and CNS-11G were added to the tested wells to make a final concentration of 1% DMSO, or 500 μM CNS-11, CNS-11D, or CNS-11G and 1% DMSO, in 200 μL of solution per well. Kinetic fluorescence data were collected in a microplate reader (FLUOstar Omega, BMG Labtech) at 37 °C with double orbital shaking at 700 rpm. Fluorescence measurements were recorded every 6 min with excitation and emission wavelengths of 448 and 482 nm. All samples were collected in triplicate.

Solubility Measurements

Internal standard was prepared by mixing 0.07 mg of dimethyl sulfone (99 wt % purity, Aldrich) with 0.70 mL of D_2O. Excess amount of the analyte (CNS-11, CNS-11D, or CNS-11G) was measured, and the internal standard in D_2O was added to the analyte. The solutions were then incubated at 50 °C for 60 min to ensure complete saturation of the analyte. The quantitative ^1H NMR spectra were then obtained by using standard ^1H NMR protocols. Solubility was determined according to the calculations described below.

$$S = \frac{\mathrm{mg_{std}} \times \mathrm{MW_{cpd}} \times \text{molar ratio}}{\mathrm{MW_{std}} \times 0.7\mathrm{mL}}$$

$$\text{molar ratio} = \frac{\left[\frac{I_{\mathrm{cpd}}}{\mathrm{nH_{cpd}}}\right]}{\left[\frac{I_{\mathrm{std}}}{\mathrm{nH_{std}}}\right]}$$

Animal Studies

P301S transgenic mice (Prnp-MAPT*P301S PS19Vle/J, JAX stock #008169, the Jackson Laboratory, Bar Harbor, ME) and B6C3F1/J mice (JAX stock #100010, the Jackson Laboratory) were housed in groups of up to four in individually ventilated cages under standard conditions (22 °C, 12 h light−dark cycle) receiving food and water ad libitum. All animal experiments were performed in accordance with the National Institutes of Health regulations, approved by UCLA Animal Research Committee and performed under oversight of the Division of Laboratory Animal Medicine.

Stereotaxic Seeding of Mice with Recombinant Tau-K18+ Fibrils

For in vivo studies of CNS-11, 10 two-month-old, male PS19 mice were stereotaxically injected with 1.5 μL of recombinant tau-K18+ preformed fibrils (5 μg/μL) in the right hippocampus (A/P, −2.5 mm from bregma; M/L, +2.0 mm; D/V, −1.4 mm) and right frontal cortex (A/P, +2.0 mm; M/L, +2.0 mm; D/V, −1.7 mm), as previously described.[62] In addition, 4 wild-type, age-matched B6C3F1/J mice were stereotaxically injected with vehicle (1× PBS) at the same coordinates to serve as controls. For in vivo studies of CNS-11D and CNS-11G, 15 two-month-old, male PS19 mice were stereotaxically injected bilaterally with 3 μL of recombinant tau-K18+ preformed fibrils (5 μg/μL) in the left hippocampus (A/P, −2.0 mm from bregma; M/L, −2.0 mm; D/V, −1.4 mm and −1.7 mm, 1.5 μL per depth) and the right hippocampus (A/P, −2.0 mm from bregma; M/L, +2.0 mm; D/V, −1.4 mm and −1.7 mm, 1.5 μL per depth).

https://doi.org/10.1021/acschemneuro.5c00940
ACS Chem. Neurosci. XXXX, XXX, XXX−XXX

Treatment of Mice with CNS-11, CNS-11D, or CNS-11G

For in vivo studies of CNS-11, the 10 PS19 mice were divided into two groups (n = 5 per group). Beginning 4 weeks after surgery, each group was intravenously administered with CNS-11 at a dose of 1 mg/kg by tail vein or with vehicle (1× PBS with 10% DMSO), every week for 8 weeks. The weight of each mouse was recorded weekly. The 4 wild-type, age-matched B6C3F1/J mice were intravenously administered with vehicle to serve as a control. For in vivo studies of CNS-11D and CNS-11G, the 15 PS19 mice were divided into two groups (n = 5 per group). Beginning 2 weeks after surgery, each group was intravenously administered with CNS-11D or CNS-11G at a dose of 1 mg/kg by tail vein, or with vehicle (1× PBS with 10% DMSO), every week for 8 weeks. The weight of each mouse was recorded weekly.

Barnes Maze

The maze consisted of a circular platform with 20 holes around the periphery, with an escape box attached to the bottom of one of the holes and shallow boxes attached to the bottom of the other holes. Bright light and white noise were used to motivate mice to find and enter the escape box. Visual extramaze cues were present on three walls of the room. For all trials, mice were placed individually in a cylindrical start chamber in the center of the maze for 30 s, which was then lifted to start the test. During an adaptation period, mice were guided to the escape tunnel and allowed to stay there for 30 s. During a spatial acquisition period, a total of 10 acquisition trials (two trials per day with an intertrial interval of 15 min) were performed; mice were allowed to explore the maze freely for 2 min. Each trial ended when the mouse entered the escape tunnel or after 2 min had elapsed. Mice that did not find the tunnel were guided to it. All mice were allowed to remain in the tunnel for 30 s. During the probe trial conducted 1 day after the last training trial, the escape tunnel was replaced by a shallow box and mice were allowed to explore the maze for 90 s. Animals' performances were monitored using Any-Maze Video Tracking System (Stoelting Co., Wood Dale, IL), which provided data for the acquisition parameter (latency to find the platform) and the probe trial parameters (latency to find the platform, number of entries in the target platform zone of the platform).

Euthanasia of Mice

Mice were sacrificed by overdose with pentobarbital, followed by transcardial perfusion with perfusion buffer (1× PBS with sodium vanadate, leupeptin, aprotinin, pepstatin, sodium pyrophosphate, sodium fluoride, and PMSF). For in vivo studies of CNS-11, the brain was removed and immediately frozen in liquid nitrogen and stored at −80 °C until used. For in vivo studies of CNS-11D and CNS-11G, the right hemisphere of the brain was removed and immediately frozen in liquid nitrogen and stored at −80 °C until used. The left hemisphere of the brain was removed and underwent three nights postfixation in neutral buffered formalin (Thermo Fisher Scientific), transferred to 70% EtOH, and processed and embedded in paraffin.

Western Blot Analyses

PBS-perfused unfixed brains were used for biochemical analysis by dissecting the hippocampi separately. Before analysis, the brain samples were sonicated in RIPA buffer (4 vol/g) [50 mM tris, 150 mM NaCl, 0.1% SDS, 0.5% sodium deoxycholate, 1% NP-40, 5 mM EDTA, 1 mM phenylmethylsulfonyl fluoride, 0.1% protease inhibitor mixture, and 0.5% phosphatase inhibitor (pH 8.0)] and centrifuged at 100,000g for 30 min at 4 °C. The supernatants were saved as RIPA-soluble fractions, whereas the RIPA-insoluble pellets were washed with 1 M sucrose in RIPA buffer to remove myelin and associated lipids and centrifuged at 100,000g for 30 min at 4 °C. The RIPA-insoluble pellets were then extracted in tissue (1 vol/g) with 2% SDS buffer [50 mM Tris-HCl (pH 7.6)]. The protein contents of the samples were measured using a BCA Protein Assay Kit (Pierce, Bonn, Germany) and diluted to the same concentration (500 μg/mL). Soluble and insoluble fractions were analyzed by SDS-PAGE, followed by Western blotting using an antitau antibody (1:5000; A0024, Dako). β-Actin was used as a loading control (1:2000; sc-47778, Santa Cruz Biotechnology). Bands were quantified by using ImageJ software.

Determination of Blood AST Levels as an Index of Hepatic Toxicity

Blood samples were obtained by cardiac puncture and centrifuged at 2000g for 20 min to separate the serum for collection. Activity of AST was assayed using Mouse AST enzyme-linked immunosorbent assay kits (Abcam, ab263882) according to the manufacturer's protocols.

Hematoxylin and Eosin Staining

Major organs including heart, liver, spleen, lung, and kidney (n = 2) were fixed in 4% buffered formalin saline (Sigma-Aldrich) at 4 °C overnight and then embedded in paraffin blocks. Tissue sections of 5 μm thickness were stained with hematoxylin and eosin (H&E). The morphology of the tissue was observed under a light microscope (Leica) at 20× magnification.

Immunohistochemistry

The brain tissues were embedded in paraffin and sectioned at a 10 μm thickness. Following deparaffinization, rehydration, heat-induced antigen retrieval in citrate buffer (pH 6.0), and blocking of endogenous peroxidase activity by 3% hydrogen peroxide, the sections were incubated with the antitau (1:500; AT8, monoclonal, mouse, Innogenetics) at 4 °C overnight. On the second day, followed by being washed three times in TBST, 5 min each, the sections were incubated in biotinylated antimouse secondary antibody (1:1000) in 1.5% normal serum with 3% bovine serum albumin/tris-buffered saline for 1 h at 37 °C. Immunolabeling was detected using the avidin−biotinylated HRP complex method (Elite Kit, Vector, USA) and was visualized with diaminobenzidine (Wako, Japan). Last, the sections were mounted onto coverslips using DPX mounting media (Thermo Fisher Scientific). The images were collected at 10× magnification with a digital MC170 5 MPixel Leica camera on a Nikon Eclipse E800 M microscope. Image processing and analysis were performed with ImageJ software. Macros were developed for each staining to attain a reproducible semiautomated quantification. The image files were converted to an eight-bit grayscale. A uniform threshold value of 50 (using the dark background option) was then applied before performing the "analyze particles" task to determine the percent of area covered by the positive signal.

■ ASSOCIATED CONTENT

Supporting Information

The Supporting Information is available free of charge at https://pubs.acs.org/doi/10.1021/acschemneuro.5c00940.

Pathology information for patient brain-extracted samples; determination of the solubility of CNS-11, CNS-11D, and CNS-11G; raw LC−MS/MS data and brain tissue; raw LC−MS/MS data, plasma, and chemical analogs of CNS-11 disaggregating tau fibrils from AD patients; CNS-11 and CNS-11G disaggregating tau fibrils from AD patients at concentrations lower than 500 μM; CNS-11, CNS-11D, and CNS-11G with dose-dependent toxicity in N2a cells; CNS-11, CNS-11D, and CNS-11G preventing seeding in HEK293 biosensor cells in a dose-dependent manner; CNS-11, CNS-11D, and CNS-11G preventing seeding by fibrils from multiple tauopathies in HEK293 biosensor cells; CNS-11, CNS-11D, and CNS-11G not modifying the ThT signal when mixed with K18+ in an aggregation assay; CNS-11D and CNS-11G soluble under physiologic conditions; PS19 mice not demonstrating behavioral deficits in Barnes maze; preformed fibril-seeded PS19 mice developing abundant tau pathology; eight weeks of treatment with CNS-11 causing no obvious toxicity in PS19 mice; CNS-11D and CNS-11G both reducing levels of insoluble tau

https://doi.org/10.1021/acschemneuro.5c00940
ACS Chem. Neurosci. XXXX, XXX, XXX−XXX

in PS19 mice; eight weeks of treatment with CNS-11D or CNS-11G causing no obvious toxicity in PS19 mice; and CNS-11D and CNS-11G each reducing phosphorylated tau in the hippocampus of PS19 mice (PDF)

AUTHOR INFORMATION

Corresponding Author

David S. Eisenberg − *Department of Chemistry and Biochemistry, UCLA, Los Angeles, California 90095, United States; Department of Biological Chemistry, UCLA-DOE Institute, Molecular Biology Institute, UCLA, Los Angeles, California 90,095, United States*; Phone: (310) 825-3754; Email: david@mbi.ucla.edu; Fax: (310) 206-3914

Authors

Hope Pan − *Department of Chemistry and Biochemistry, UCLA, Los Angeles, California 90095, United States; Department of Biological Chemistry, UCLA-DOE Institute, Molecular Biology Institute, UCLA, Los Angeles, California 90,095, United States*; orcid.org/0000-0001-6509-6224

Xinyi Cheng − *Department of Chemistry and Biochemistry, UCLA, Los Angeles, California 90095, United States; Department of Biological Chemistry, UCLA-DOE Institute, Molecular Biology Institute, UCLA, Los Angeles, California 90,095, United States*

Jeffrey Zhang − *Department of Chemistry and Biochemistry, UCLA, Los Angeles, California 90095, United States; Department of Biological Chemistry, UCLA-DOE Institute, Molecular Biology Institute, UCLA, Los Angeles, California 90,095, United States*

Ke Hou − *Department of Chemistry and Biochemistry, UCLA, Los Angeles, California 90095, United States; Department of Biological Chemistry, UCLA-DOE Institute, Molecular Biology Institute, UCLA, Los Angeles, California 90,095, United States*

Kevin A. Murray − *Department of Chemistry and Biochemistry, UCLA, Los Angeles, California 90095, United States; Department of Biological Chemistry, UCLA-DOE Institute, Molecular Biology Institute, UCLA, Los Angeles, California 90,095, United States; Department of Neurology, Brown University, Providence, Rhode Island 02912, United States*

Kapil Manglani − *Geriatric Research Education and Clinical Center, Greater Los Angeles Veterans Affairs Healthcare System, West Los Angeles VA Medical Center, Los Angeles, California 90073, United States; Department of Neurology and Department of Medicine, David Geffen School of Medicine at UCLA, Los Angeles, California 90095, United States*

Cansheng Zhu − *Geriatric Research Education and Clinical Center, Greater Los Angeles Veterans Affairs Healthcare System, West Los Angeles VA Medical Center, Los Angeles, California 90073, United States; Department of Neurology and Department of Medicine, David Geffen School of Medicine at UCLA, Los Angeles, California 90095, United States*

Hung-Kai Hsu − *Department of Chemistry and Biochemistry, UCLA, Los Angeles, California 90095, United States*; orcid.org/0000-0001-9347-2290

Marisa Mekkittikul − *Geriatric Research Education and Clinical Center, Greater Los Angeles Veterans Affairs Healthcare System, West Los Angeles VA Medical Center, Los Angeles, California 90073, United States; Department of Neurology and Department of Medicine, David Geffen School of Medicine at UCLA, Los Angeles, California 90095, United States*

Tyler Halladay − *Department of Chemistry and Biochemistry, UCLA, Los Angeles, California 90095, United States; Department of Biological Chemistry, UCLA-DOE Institute, Molecular Biology Institute, UCLA, Los Angeles, California 90,095, United States*

Hilda Mirbaha − *Department of Pathology and Laboratory Medicine, David Geffen School of Medicine, UCLA, Los Angeles, California 90095, United States*

Gazmend Elezi − *Pasarow Mass Spectrometry Laboratory, David Geffen School of Medicine, UCLA, Los Angeles, California 90095, United States*

Romany Abskharon − *Department of Chemistry and Biochemistry, UCLA, Los Angeles, California 90095, United States; Department of Biological Chemistry, UCLA-DOE Institute, Molecular Biology Institute, UCLA, Los Angeles, California 90,095, United States*

Michael R. Sawaya − *Department of Chemistry and Biochemistry, UCLA, Los Angeles, California 90095, United States; Department of Biological Chemistry, UCLA-DOE Institute, Molecular Biology Institute, UCLA, Los Angeles, California 90,095, United States*; orcid.org/0000-0003-0874-9043

Alexander Bombino − *Geriatric Research Education and Clinical Center, Greater Los Angeles Veterans Affairs Healthcare System, West Los Angeles VA Medical Center, Los Angeles, California 90073, United States; Department of Neurology and Department of Medicine, David Geffen School of Medicine at UCLA, Los Angeles, California 90095, United States*

Christopher K. Williams − *Department of Neurology, David Geffen School of Medicine at UCLA, Los Angeles, California 90095, United States; Department of Pathology and Laboratory Medicine, David Geffen School of Medicine, UCLA, Los Angeles, California 90095, United States*

Michael DeTure − *Department of Neuroscience, Mayo Clinic, Jacksonville, Florida 32224, United States*

Dennis W. Dickson − *Department of Neuroscience, Mayo Clinic, Jacksonville, Florida 32224, United States*

Harry V. Vinters − *Department of Neurology, David Geffen School of Medicine at UCLA, Los Angeles, California 90095, United States; Department of Pathology and Laboratory Medicine, David Geffen School of Medicine, UCLA, Los Angeles, California 90095, United States*

Julian P. Whitelegge − *Department of Pathology and Laboratory Medicine, David Geffen School of Medicine, UCLA, Los Angeles, California 90095, United States*; orcid.org/0000-0003-2763-7733

Patrick G. Harran − *Department of Chemistry and Biochemistry, UCLA, Los Angeles, California 90095, United States*; orcid.org/0000-0001-8748-5167

Gregory M. Cole − *Geriatric Research Education and Clinical Center, Greater Los Angeles Veterans Affairs Healthcare System, West Los Angeles VA Medical Center, Los Angeles, California 90073, United States; Department of Neurology and Department of Medicine, David Geffen School of Medicine at UCLA, Los Angeles, California 90095, United States*

Sally A. Frautschy − *Geriatric Research Education and Clinical Center, Greater Los Angeles Veterans Affairs*

https://doi.org/10.1021/acschemneuro.5c00940
ACS Chem. Neurosci. XXXX, XXX, XXX−XXX

Healthcare System, West Los Angeles VA Medical Center, Los Angeles, California 90073, United States; Department of Neurology and Department of Medicine, David Geffen School of Medicine at UCLA, Los Angeles, California 90095, United States

Complete contact information is available at: https://pubs.acs.org/10.1021/acschemneuro.5c00940

Author Contributions

♦H.P., X.C., and J.Z. contributed equally. K.A.M. designed chemical analogs of CNS-11. X.C., J.Z., and H.H. performed ex vivo characterization of chemical analogs. H.P., K.H., K.M., C.Z., M.M., T.H., G.E., R.A., and A.B. performed animal experiments. H.P., X.C., J.Z., H.M., M.R.S., P.G.H., J.P.W., G.M.C., and S.A.F. analyzed data; C.K.W., M.D., D.W.D., and H.V.V. contributed patient brain samples; H.P., X.C., J.Z., and D.S.E. wrote the manuscript with contributions from all other authors.

Notes

The authors declare the following competing financial interest(s): DSE is SAB chair and equity holder in ADRx, Inc.

■ ACKNOWLEDGMENTS

We thank the donors and their families without whom this work would not have been possible. Research reported in this publication was supported by 1R01AG070895 (D.S.E.) and R01 AG048120 (D.S.E.) and NIH/National Center for Advancing Translational Science (NCATS) UCLA CTSI Grant Number UL1TR001881 (H.P. and D.S.E.). H.P. is supported by the UCLA-Caltech Medical Scientist Training Program (NIGMS T32 GM008042), the UCLA Chemistry-Biology Interface Training Grant (5T32GM008496), and the Ruth L. Kirschstein National Research Service Award (1F30AG077832-01A1). We thank Marc Diamond from UT Southwestern for the generous gift of biosensor cells. We thank the UCLA Behavior Testing Core for assistance with behavior testing. We thank the UCLA Translational Pathology Core Laboratory for assistance in paraffin-embedding mouse brain tissue.

■ REFERENCES

(1) van Dyck, C. H.; Swanson, C. J.; Aisen, P.; Bateman, R. J.; Chen, C.; Gee, M.; Kanekiyo, M.; Li, D.; Reyderman, L.; Cohen, S.; Froelich, L.; Katayama, S.; Sabbagh, M.; Vellas, B.; Watson, D.; Dhadda, S.; Irizarry, M.; Kramer, L. D.; Iwatsubo, T. Lecanemab in Early Alzheimer's Disease. *N. Engl. J. Med.* **2023**, *388* (1), 9−21.

(2) Sims, J. R.; Zimmer, J. A.; Evans, C. D.; Lu, M.; Ardayfio, P.; Sparks, J.; Wessels, A. M.; Shcherbinin, S.; Wang, H.; Monkul Nery, E. S.; Collins, E. C.; Solomon, P.; Salloway, S.; Apostolova, L. G.; Hansson, O.; Ritchie, C.; Brooks, D. A.; Mintun, M.; Skovronsky, D. M.; et al. TRAILBLAZER-ALZ 2 Investigators. Donanemab in Early Symptomatic Alzheimer Disease: The TRAILBLAZER-ALZ 2 Randomized Clinical Trial. *JAMA* **2023**, *330* (6), 512−527.

(3) Cho, H.; Choi, J. Y.; Hwang, M. S.; Lee, J. H.; Kim, Y. J.; Lee, H. M.; Lyoo, C. H.; Ryu, Y. H.; Lee, M. S. Tau PET in Alzheimer Disease and Mild Cognitive Impairment. *Neurology* **2016**, *87* (4), 375−383.

(4) Wang, L.; Benzinger, T. L.; Su, Y.; Christensen, J.; Friedrichsen, K.; Aldea, P.; McConathy, J.; Cairns, N. J.; Fagan, A. M.; Morris, J. C.; Ances, B. M. Evaluation of Tau Imaging in Staging Alzheimer Disease and Revealing Interactions Between β-Amyloid and Tauopathy. *JAMA Neurol.* **2016**, *73* (9), 1070−1077.

(5) Xia, C.; Makaretz, S. J.; Caso, C.; McGinnis, S.; Gomperts, S. N.; Sepulcre, J.; Gomez-Isla, T.; Hyman, B. T.; Schultz, A.; Vasdev, N.; Johnson, K. A.; Dickerson, B. C. Association of In Vivo [18F]AV-1451 Tau PET Imaging Results With Cortical Atrophy and Symptoms in Typical and Atypical Alzheimer Disease. *JAMA Neurol.* **2017**, *74* (4), 427−436.

(6) La Joie, R.; Visani, A. V.; Baker, S. L.; Brown, J. A.; Bourakova, V.; Cha, J.; Chaudhary, K.; Edwards, L.; Iaccarino, L.; Janabi, M.; Lesman-Segev, O. H.; Miller, Z. A.; Perry, D. C.; O'Neil, J. P.; Pham, J.; Rojas, J. C.; Rosen, H. J.; Seeley, W. W.; Tsai, R. M.; Miller, B. L.; Jagust, W. J.; Rabinovici, G. D. Prospective Longitudinal Atrophy in Alzheimer's Disease Correlates with the Intensity and Topography of Baseline Tau-PET. *Sci. Transl. Med.* **2020**, *12* (524), No. eaau5732.

(7) Arriagada, P. V.; Growdon, J. H.; Hedley-Whyte, E. T.; Hyman, B. T. Neurofibrillary Tangles but Not Senile Plaques Parallel Duration and Severity of Alzheimer's Disease. *Neurology* **1992**, *42* (3), 631.

(8) Gómez-Isla, T.; Hollister, R.; West, H.; Mui, S.; Growdon, J. H.; Petersen, R. C.; Parisi, J. E.; Hyman, B. T. Neuronal Loss Correlates with but Exceeds Neurofibrillary Tangles in Alzheimer's Disease. *Ann. Neurol.* **1997**, *41* (1), 17−24.

(9) Giannakopoulos, P.; Herrmann, F. R.; Bussière, T.; Bouras, C.; Kövari, E.; Perl, D. P.; Morrison, J. H.; Gold, G.; Hof, P. R. Tangle and Neuron Numbers, but Not Amyloid Load, Predict Cognitive Status in Alzheimer's Disease. *Neurology* **2003**, *60* (9), 1495−1500.

(10) Bennett, D. A.; Schneider, J. A.; Wilson, R. S.; Bienias, J. L.; Arnold, S. E. Neurofibrillary Tangles Mediate the Association of Amyloid Load With Clinical Alzheimer Disease and Level of Cognitive Function. *Arch. Neurol.* **2004**, *61* (3), 378−384.

(11) Haroutunian, V.; Davies, P.; Vianna, C.; Buxbaum, J. D.; Purohit, D. P. Tau Protein Abnormalities Associated with the Progression of Alzheimer Disease Type Dementia. *Neurobiol. Aging* **2007**, *28* (1), 1−7.

(12) Braak, H.; Braak, E. Neuropathological Stageing of Alzheimer-Related Changes. *Acta Neuropathol.* **1991**, *82* (4), 239−259.

(13) Braak, H.; Braak, E. Staging of Alzheimer's Disease-Related Neurofibrillary Changes. *Neurobiol. Aging* **1995**, *16* (3), 271−278.

(14) Frost, B.; Ollesch, J.; Wille, H.; Diamond, M. I. Conformational Diversity of Wild-Type Tau Fibrils Specified by Templated Conformation Change. *J. Biol. Chem.* **2009**, *284* (6), 3546−3551.

(15) Frost, B.; Jacks, R. L.; Diamond, M. I. Propagation of Tau Misfolding from the Outside to the Inside of a Cell. *J. Biol. Chem.* **2009**, *284* (19), 12845−12852.

(16) Guo, J. L.; Lee, V. M.-Y. Seeding of Normal Tau by Pathological Tau Conformers Drives Pathogenesis of Alzheimer-like Tangles. *J. Biol. Chem.* **2011**, *286* (17), 15317−15331.

(17) Holmes, B. B.; Furman, J. L.; Mahan, T. E.; Yamasaki, T. R.; Mirbaha, H.; Eades, W. C.; Belaygorod, L.; Cairns, N. J.; Holtzman, D. M.; Diamond, M. I. Proteopathic Tau Seeding Predicts Tauopathy in Vivo. *Proc. Natl. Acad. Sci. U.S.A.* **2014**, *111* (41), E4376−E4385.

(18) Clavaguera, F.; Bolmont, T.; Crowther, R. A.; Abramowski, D.; Frank, S.; Probst, A.; Fraser, G.; Stalder, A. K.; Beibel, M.; Staufenbiel, M.; Jucker, M.; Goedert, M.; Tolnay, M. Transmission and Spreading of Tauopathy in Transgenic Mouse Brain. *Nat. Cell Biol.* **2009**, *11* (7), 909−913.

(19) Clavaguera, F.; Akatsu, H.; Fraser, G.; Crowther, R. A.; Frank, S.; Hench, J.; Probst, A.; Winkler, D. T.; Reichwald, J.; Staufenbiel, M.; Ghetti, B.; Goedert, M.; Tolnay, M. Brain Homogenates from Human Tauopathies Induce Tau Inclusions in Mouse Brain. *Proc. Natl. Acad. Sci. U.S.A.* **2013**, *110* (23), 9535−9540.

(20) Iba, M.; Guo, J. L.; McBride, J. D.; Zhang, B.; Trojanowski, J. Q.; Lee, V. M.-Y. Synthetic Tau Fibrils Mediate Transmission of Neurofibrillary Tangles in a Transgenic Mouse Model of Alzheimer's-Like Tauopathy. *J. Neurosci.* **2013**, *33* (3), 1024−1037.

(21) Boluda, S.; Iba, M.; Zhang, B.; Raible, K. M.; Lee, V. M.-Y.; Trojanowski, J. Q. Differential Induction and Spread of Tau Pathology in Young PS19 Tau Transgenic Mice Following Intracerebral Injections of Pathological Tau from Alzheimer's Disease or Corticobasal Degeneration Brains. *Acta Neuropathol.* **2015**, *129* (2), 221−237.

(22) Guo, J. L.; Narasimhan, S.; Changolkar, L.; He, Z.; Stieber, A.; Zhang, B.; Gathagan, R. J.; Iba, M.; McBride, J. D.; Trojanowski, J. Q.;

Lee, V. M. Y. Unique Pathological Tau Conformers from Alzheimer's Brains Transmit Tau Pathology in Nontransgenic Mice. *J. Exp. Med.* **2016**, *213* (12), 2635−2654.
(23) Narasimhan, S.; Guo, J. L.; Changolkar, L.; Stieber, A.; McBride, J. D.; Silva, L. V.; He, Z.; Zhang, B.; Gathagan, R. J.; Trojanowski, J. Q.; Lee, V. M. Y. Pathological Tau Strains from Human Brains Recapitulate the Diversity of Tauopathies in Nontransgenic Mouse Brain. *J. Neurosci.* **2017**, *37* (47), 11406−11423.
(24) Ehrnhoefer, D. E.; Bieschke, J.; Boeddrich, A.; Herbst, M.; Masino, L.; Lurz, R.; Engemann, S.; Pastore, A.; Wanker, E. E. EGCG Redirects Amyloidogenic Polypeptides into Unstructured, off-Pathway Oligomers. *Nat. Struct. Mol. Biol.* **2008**, *15* (6), 558−566.
(25) Bieschke, J.; Russ, J.; Friedrich, R. P.; Ehrnhoefer, D. E.; Wobst, H.; Neugebauer, K.; Wanker, E. E. EGCG Remodels Mature α-Synuclein and Amyloid-β Fibrils and Reduces Cellular Toxicity. *Proc. Natl. Acad. Sci. U.S.A.* **2010**, *107* (17), 7710−7715.
(26) Sonawane, S. K.; Chidambaram, H.; Boral, D.; Gorantla, N. V.; Balmik, A. A.; Dangi, A.; Ramasamy, S.; Marelli, U. K.; Chinnathambi, S. EGCG Impedes Human Tau Aggregation and Interacts with Tau. *Sci. Rep.* **2020**, *10* (1), 12579.
(27) Andreu Fernández, V.; Almeida Toledano, L.; Pizarro Lozano, N.; Navarro Tapia, E.; Gómez Roig, M. D.; De la Torre Fornell, R.; García Algar, Ó. Bioavailability of Epigallocatechin Gallate Administered with Different Nutritional Strategies in Healthy Volunteers. *Antioxidants* **2020**, *9* (5), 440.
(28) Seidler, P. M.; Murray, K. A.; Boyer, D. R.; Ge, P.; Sawaya, M. R.; Hu, C. J.; Cheng, X.; Abskharon, R.; Pan, H.; DeTure, M. A.; Williams, C. K.; Dickson, D. W.; Vinters, H. V.; Eisenberg, D. S. Structure-Based Discovery of Small Molecules That Disaggregate Alzheimer's Disease Tissue Derived Tau Fibrils in Vitro. *Nat. Commun.* **2022**, *13* (1), 5451.
(29) Murray, K. A.; Hu, C. J.; Pan, H.; Lu, J.; Abskharon, R.; Bowler, J. T.; Rosenberg, G. M.; Williams, C. K.; Elezi, G.; Balbirnie, M.; Faull, K. F.; Vinters, H. V.; Seidler, P. M.; Eisenberg, D. S. Small Molecules Disaggregate Alpha-Synuclein and Prevent Seeding from Patient Brain-Derived Fibrils. *Proc. Natl. Acad. Sci. U.S.A.* **2023**, *120* (7), No. e2217835120.
(30) Yoshiyama, Y.; Higuchi, M.; Zhang, B.; Huang, S.-M.; Iwata, N.; Saido, T. C.; Maeda, J.; Suhara, T.; Trojanowski, J. Q.; Lee, V. M.-Y. Synapse Loss and Microglial Activation Precede Tangles in a P301S Tauopathy Mouse Model. *Neuron* **2007**, *53* (3), 337−351.
(31) Peeraer, E.; Bottelbergs, A.; Van Kolen, K.; Stancu, I.-C.; Vasconcelos, B.; Mahieu, M.; Duytschaever, H.; Ver Donck, L.; Torremans, A.; Sluydts, E.; Van Acker, N.; Kemp, J. A.; Mercken, M.; Brunden, K. R.; Trojanowski, J. Q.; Dewachter, I.; Lee, V. M. Y.; Moechars, D. Intracerebral Injection of Preformed Synthetic Tau Fibrils Initiates Widespread Tauopathy and Neuronal Loss in the Brains of Tau Transgenic Mice. *Neurobiol. Dis.* **2015**, *73*, 83−95.
(32) Takeuchi, H.; Iba, M.; Inoue, H.; Higuchi, M.; Takao, K.; Tsukita, K.; Karatsu, Y.; Iwamoto, Y.; Miyakawa, T.; Suhara, T.; Trojanowski, J. Q.; Lee, V. M.-Y.; Takahashi, R. P301S Mutant Human Tau Transgenic Mice Manifest Early Symptoms of Human Tauopathies with Dementia and Altered Sensorimotor Gating. *PLoS One* **2011**, *6* (6), No. e21050.
(33) Congdon, E. E.; Ji, C.; Tetlow, A. M.; Jiang, Y.; Sigurdsson, E. M. Tau-Targeting Therapies for Alzheimer Disease: Current Status and Future Directions. *Nat. Rev. Neurol.* **2023**, *19* (12), 715−736.
(34) Theunis, C.; Crespo-Biel, N.; Gafner, V.; Pihlgren, M.; López-Deber, M. P.; Reis, P.; Hickman, D. T.; Adolfsson, O.; Chuard, N.; Ndao, D. M.; Borghgraef, P.; Devijver, H.; Van Leuven, F.; Pfeifer, A.; Muhs, A. Efficacy and Safety of A Liposome-Based Vaccine against Protein Tau, Assessed in Tau.P301L Mice That Model Tauopathy. *PLoS One* **2013**, *8* (8), No. e72301.
(35) Gauthier, S.; Feldman, H. H.; Schneider, L. S.; Wilcock, G. K.; Frisoni, G. B.; Hardlund, J. H.; Moebius, H. J.; Bentham, P.; Kook, K. A.; Wischik, D. J.; Schelter, B. O.; Davis, C. S.; Staff, R. T.; Bracoud, L.; Shamsi, K.; Storey, J. M. D.; Harrington, C. R.; Wischik, C. M. Efficacy and Safety of Tau-Aggregation Inhibitor Therapy in Patients with Mild or Moderate Alzheimer's Disease: A Randomised, Controlled, Double-Blind, Parallel-Arm, Phase 3 Trial. *Lancet* **2016**, *388* (10062), 2873−2884.
(36) Wilcock, G. K.; Gauthier, S.; Frisoni, G. B.; Jia, J.; Hardlund, J. H.; Moebius, H. J.; Bentham, P.; Kook, K. A.; Schelter, B. O.; Wischik, D. J.; Davis, C. S.; Staff, R. T.; Vesna, V.; Trevor, A.; Luc, B.; Kohkan, S.; Ken, M.; John, S.; Gernot, R.; John, M. D. S.; Charles, H. R.; Claude, W. M. Potential of Low Dose Leuco-Methylthioninium Bis(Hydromethanesulphonate) (LMTM) Monotherapy for Treatment of Mild Alzheimer's Disease: Cohort Analysis as Modified Primary Outcome in a Phase III Clinical Trial. *J. Alzheimers Dis.* **2018**, *61*, 435.
(37) Shiells, H.; Schelter, B. O.; Bentham, P.; Baddeley, T. C.; Rubino, C. M.; Ganesan, H.; Hammel, J.; Vuksanovic, V.; Staff, R. T.; Murray, A. D.; Bracoud, L.; Wischik, D. J.; Riedel, G.; Gauthier, S.; Jia, J.; Moebius, H. J.; Hardlund, J.; Kipps, C. M.; Kook, K.; Storey, J. M. D.; Harrington, C. R.; Wischik, C. M. Concentration-Dependent Activity of Hydromethylthionine on Clinical Decline and Brain Atrophy in a Randomized Controlled Trial in Behavioral Variant Frontotemporal Dementia. *J Alzheimers Dis.* **2020**, *75*, 501−519.
(38) Wischik, C. M.; Bentham, P.; Gauthier, S.; Miller, S.; Kook, K.; Schelter, B. O. Oral Tau Aggregation Inhibitor for Alzheimer's Disease: Design, Progress and Basis for Selection of the 16 Mg/Day Dose in a Phase 3, Randomized, Placebo-Controlled Trial of Hydromethylthionine Mesylate. *J. Prev. Alzheimers Dis.* **2022**, *9* (4), 780−790.
(39) Schelter, B. O.; Shiells, H.; Baddeley, T. C.; Rubino, C. M.; Ganesan, H.; Hammel, J.; Vuksanovic, V.; Staff, R. T.; Murray, A. D.; Bracoud, L.; Riedel, G.; Gauthier, S.; Jia, J.; Bentham, P.; Kook, K.; Storey, J. M. D.; Harrington, C. R.; Wischik, C. M. Concentration-Dependent Activity of Hydromethylthionine on Cognitive Decline and Brain Atrophy in Mild to Moderate Alzheimer's Disease. *J. Alzheimer's Dis.* **2019**, *72* (3), 931−946.
(40) Ross, E. L.; Weinberg, M. S.; Arnold, S. E. Cost-Effectiveness of Aducanumab and Donanemab for Early Alzheimer Disease in the US. *JAMA Neurol* **2022**, *79* (5), 478−487.
(41) Jeremic, D.; Navarro-López, J. D.; Jiménez-Díaz, L. Donanemab Outperformed Aducanumab and Lecanemab on Cognitive, but Not on Biomarker and Safety Outcomes: Systematic Review, Frequentist and Bayesian Network Meta-Analyses. *medRxiv* **2024**, 2024.03.31.24305134.
(42) Beck, H.; Härter, M.; Haß, B.; Schmeck, C.; Baerfacker, L. Small Molecules and Their Impact in Drug Discovery: A Perspective on the Occasion of the 125th Anniversary of the Bayer Chemical Research Laboratory. *Drug Discovery Today* **2022**, *27* (6), 1560−1574.
(43) Lo, C. H.; Lim, C. K.-W.; Ding, Z.; Wickramasinghe, S. P.; Braun, A. R.; Ashe, K. H.; Rhoades, E.; Thomas, D. D.; Sachs, J. N. Targeting the Ensemble of Heterogeneous Tau Oligomers in Cells: A Novel Small Molecule Screening Platform for Tauopathies. *Alzheimers Dement.* **2019**, *15* (11), 1489−1502.
(44) Singh, G.; Liu, P.; Yao, K. R.; Strasser, J. M.; Hlynialuk, C.; Leinonen-Wright, K.; Teravskis, P. J.; Choquette, J. M.; Ikramuddin, J.; Bresinsky, M.; Nelson, K. M.; Liao, D.; Ashe, K. H.; Walters, M. A.; Pockes, S. Caspase-2 Inhibitor Blocks Tau Truncation and Restores Excitatory Neurotransmission in Neurons Modeling FTDP-17 Tauopathy. *ACS Chem. Neurosci.* **2022**, *13* (10), 1549−1557.
(45) Taniguchi, S.; Suzuki, N.; Masuda, M.; Hisanaga, S.; Iwatsubo, T.; Goedert, M.; Hasegawa, M. Inhibition of Heparin-Induced Tau Filament Formation by Phenothiazines, Polyphenols, and Porphyrins. *J. Biol. Chem.* **2005**, *280* (9), 7614−7623.
(46) Wischik, C. M.; Edwards, P. C.; Lai, R. Y.; Roth, M.; Harrington, C. R. Selective Inhibition of Alzheimer Disease-like Tau Aggregation by Phenothiazines. *Proc. Natl. Acad. Sci. U.S.A.* **1996**, *93* (20), 11213−11218.
(47) Melis, V.; Magbagbeolu, M.; Rickard, J. E.; Horsley, D.; Davidson, K.; Harrington, K. A.; Goatman, K.; Goatman, E. A.; Deiana, S.; Close, S. P.; Zabke, C.; Stamer, K.; Dietze, S.; Schwab, K.; Storey, J. M. D.; Harrington, C. R.; Wischik, C. M.; Theuring, F.;

https://doi.org/10.1021/acschemneuro.5c00940
ACS Chem. Neurosci. XXXX, XXX, XXX−XXX

Riedel, G. Effects of Oxidized and Reduced Forms of Methylthioninium in Two Transgenic Mouse Tauopathy Models. *Behav. Pharmacol.* **2015**, *26* (4), 353.
(48) Schelter, B. O.; Shiells, H.; Baddeley, T. C.; Rubino, C. M.; Ganesan, H.; Hammel, J.; Vuksanovic, V.; Staff, R. T.; Murray, A. D.; Bracoud, L.; Riedel, G.; Gauthier, S.; Jia, J.; Bentham, P.; Kook, K.; Storey, J. M. D.; Harrington, C. R.; Wischik, C. M. Concentration-Dependent Activity of Hydromethylthionine on Cognitive Decline and Brain Atrophy in Mild to Moderate Alzheimer's Disease. *J. Alzheimer's Dis.* **2019**, *72* (3), 931−946.
(49) Nachman, E.; Wentink, A. S.; Madiona, K.; Bousset, L.; Katsinelos, T.; Allinson, K.; Kampinga, H.; McEwan, W. A.; Jahn, T. R.; Melki, R.; Mogk, A.; Bukau, B.; Nussbaum-Krammer, C. Disassembly of Tau Fibrils by the Human Hsp70 Disaggregation Machinery Generates Small Seeding-Competent Species. *J. Biol. Chem.* **2020**, *295* (28), 9676−9690.
(50) Dishino, D. D.; Welch, M. J.; Kilbourn, M. R.; Raichle, M. E. Relationship Between Lipophilicity and Brain Extraction of C-11-Labeled Radiopharmaceuticals. *J. Nucl. Med.* **1983**, *24* (11), 1030−1038.
(51) Levin, V. A. Relationship of Octanol/Water Partition Coefficient and Molecular Weight to Rat Brain Capillary Permeability. *J. Med. Chem.* **1980**, *23* (6), 682−684.
(52) Shi, Y.; Zhang, W.; Yang, Y.; Murzin, A. G.; Falcon, B.; Kotecha, A.; van Beers, M.; Tarutani, A.; Kametani, F.; Garringer, H. J.; Vidal, R.; Hallinan, G. I.; Lashley, T.; Saito, Y.; Murayama, S.; Yoshida, M.; Tanaka, H.; Kakita, A.; Ikeuchi, T.; Robinson, A. C.; Mann, D. M. A.; Kovacs, G. G.; Revesz, T.; Ghetti, B.; Hasegawa, M.; Goedert, M.; Scheres, S. H. W. Structure-Based Classification of Tauopathies. *Nature* **2021**, *598* (7880), 359−363.
(53) Schweighauser, M.; Murzin, A. G.; Macdonald, J.; Lavenir, I.; Crowther, R. A.; Scheres, S. H. W.; Goedert, M. Cryo-EM Structures of Tau Filaments from the Brains of Mice Transgenic for Human Mutant P301S Tau. *Acta Neuropathol. Commun.* **2023**, *11* (1), 160.
(54) Zhang, W.; Falcon, B.; Murzin, A. G.; Fan, J.; Crowther, R. A.; Goedert, M.; Scheres, S. H. Heparin-Induced Tau Filaments Are Polymorphic and Differ from Those in Alzheimer's and Pick's Diseases. *eLife* **2019**, *8*, No. e43584.
(55) Wager, T. T.; Hou, X.; Verhoest, P. R.; Villalobos, A. Moving beyond Rules: The Development of a Central Nervous System Multiparameter Optimization (CNS MPO) Approach To Enable Alignment of Druglike Properties. *ACS Chem. Neurosci.* **2010**, *1* (6), 435−449.
(56) Brendel, M.; Deussing, M.; Blume, T.; Kaiser, L.; Probst, F.; Overhoff, F.; Peters, F.; von Ungern-Sternberg, B.; Ryazanov, S.; Leonov, A.; Griesinger, C.; Zwergal, A.; Levin, J.; Bartenstein, P.; Yakushev, I.; Cumming, P.; Boening, G.; Ziegler, S.; Herms, J.; Giese, A.; Rominger, A. Late-Stage Anle138b Treatment Ameliorates Tau Pathology and Metabolic Decline in a Mouse Model of Human Alzheimer's Disease Tau. *Alzheimers Res. Ther.* **2019**, *11* (1), 67.
(57) Wegrzynowicz, M.; Bar-On, D.; Calo', L.; Anichtchik, O.; Iovino, M.; Xia, J.; Ryazanov, S.; Leonov, A.; Giese, A.; Dalley, J. W.; Griesinger, C.; Ashery, U.; Spillantini, M. G. Depopulation of Dense α-Synuclein Aggregates Is Associated with Rescue of Dopamine Neuron Dysfunction and Death in a New Parkinson's Disease Model. *Acta Neuropathol.* **2019**, *138* (4), 575−595.
(58) Cuddy, L. K.; Alia, A. O.; Salvo, M. A.; Chandra, S.; Grammatopoulos, T. N.; Justman, C. J.; Lansbury, P. T.; Mazzulli, J. R.; Vassar, R. Farnesyltransferase Inhibitor LNK-754 Attenuates Axonal Dystrophy and Reduces Amyloid Pathology in Mice. *Mol. Neurodegener.* **2022**, *17* (1), 54.
(59) Falcon, B.; Zhang, W.; Schweighauser, M.; Murzin, A. G.; Vidal, R.; Garringer, H. J.; Ghetti, B.; Scheres, S. H. W.; Goedert, M. Tau Filaments from Multiple Cases of Sporadic and Inherited Alzheimer's Disease Adopt a Common Fold. *Acta Neuropathol.* **2018**, *136* (5), 699−708.
(60) Fitzpatrick, A. W. P.; Falcon, B.; He, S.; Murzin, A. G.; Murshudov, G.; Garringer, H. J.; Crowther, R. A.; Ghetti, B.; Goedert, M.; Scheres, S. H. W. Cryo-EM Structures of Tau Filaments from Alzheimer's Disease. *Nature* **2017**, *547* (7662), 185−190.
(61) Hou, K.; Pan, H.; Shahpasand-Kroner, H.; Hu, C.; Abskharon, R.; Seidler, P.; Mekkittikul, M.; Balbirnie, M.; Lantz, C.; Sawaya, M. R.; Dolinsky, J. L.; Jones, M.; Zuo, X.; Loo, J. A.; Frautschy, S.; Cole, G.; Eisenberg, D. S. D-Peptide-Magnetic Nanoparticles Fragment Tau Fibrils and Rescue Behavioral Deficits in a Mouse Model of Alzheimer's Disease. *Sci. Adv.* **2024**, *10* (18), No. eadl2991.
(62) Peeraer, E.; Bottelbergs, A.; Van Kolen, K.; Stancu, I.-C.; Vasconcelos, B.; Mahieu, M.; Duytschaever, H.; Ver Donck, L.; Torremans, A.; Sluydts, E.; Van Acker, N.; Kemp, J. A.; Mercken, M.; Brunden, K. R.; Trojanowski, J. Q.; Dewachter, I.; Lee, V. M. Y.; Moechars, D. Intracerebral Injection of Preformed Synthetic Tau Fibrils Initiates Widespread Tauopathy and Neuronal Loss in the Brains of Tau Transgenic Mice. *Neurobiol. Dis.* **2015**, *73*, 83−95.

https://doi.org/10.1021/acschemneuro.5c00940
ACS Chem. Neurosci. XXXX, XXX, XXX−XXX